Thesis for the Degree of Doctor of Philosophy

Evaluation of Sigma-Delta-over-Fiber for High-Speed Wireless Applications

Ibrahim Can Sezgin

CHALMERS

Microwave Electronics Laboratory
Department of Microtechnology and Nanoscience – MC2
Chalmers University of Technology
Göteborg, Sweden 2020

Evaluation of Sigma-Delta-over-Fiber for High-Speed Wireless Applications

Ibrahim Can Sezgin

ISBN 978-91-7905-408-3

Doktorsavhandlingar vid Chalmers tekniska högskola.
Ny serie nr 4875
ISSN 0346-718X

Chalmers University of Technology
Department of Microtechnology and Nanoscience – MC2
Microwave Electronics Laboratory
SE-412 96 Göteborg, Sweden
+ 46 (0) 31-772 1000

Printed by Chalmers Reproservice
Göteborg, Sweden 2020

Abstract

Future mobile communication networks aim to increase the communication speed, provide better reliability and improve the coverage. They need to achieve all of these enhancements, while the number of users are increasing drastically. As a result, new base-station (BS) architectures where the signal processing is centralized and wireless access is provided through multiple, carefully coordinated remote radio heads are needed. Sigma-delta-over-fiber (SDoF) is a communication technique that can address both requirements, and enable very low-complexity, phase coherent remote radio transmission, while transmitting wide-band communication signals with high quality. This thesis investigates the potential and limitations of SDoF communication links as an enabler for future mobile networks.

In the first part of the thesis, an ultra-high-speed SDoF (UHS-SDoF) link is realized by using state-of-the-art vertical-cavity surface-emitting-lasers (VCSEL). The effects of VCSEL characteristics on such links in terms of signal quality, energy efficiency and potential lifespan is investigated. Furthermore, the potential and limitations of UHS-SDoF are evaluated with signals having various parameters. The results show that, low-cost, reliable, energy efficient, high signal quality SDoF links can be formed by using emerging VCSEL technology. Therefore, ultra-high-speed SDoF is a very promising technique for beyond 10 GHz communication systems.

In the second part of the thesis, a multiple-input-multiple-output (MIMO) communication testbed with physically separated antenna elements, distributed-MIMO, is formed by multiple SDoF links. It is shown that the digital up-conversion, performed with a shared local-oscillator/clock at the central unit, provides excellent phase coherency between the physically distributed antenna elements. The proposed testbed demonstrates the advantages of SDoF for realizing distributed MIMO systems and is a powerful tool to perform various communication experiments in real environments.

In general, SDoF is a solution for the downlink of a communication system, i.e. from central unit to remote radio head, however, the low complexity and low cost requirement of the remote radio heads makes it difficult to realize the uplinks in such systems. The third part of this thesis proposes an all-digital solution for realizing complementary uplinks for SDoF systems. The proposed structure is extensively investigated through simulations and measurements and the results demonstrate that it is possible realize all-digital, time-division duplex, optical communication links between central units and remote radio heads.

In summary, the results in this thesis demonstrate the potential of SDoF

for wideband, distributed MIMO communication systems and proposes a new architecture for all-digital duplex communication links. Overall, the thesis shows that SDoF technique is powerful technique for emerging and future mobile communication networks, since it enables a centralized structure with low complexity remote radio heads and provides high signal quality.

Keywords: Sigma-delta-over-fiber (SDoF), distributed-MIMO, vertical-cavity surface-emitting-laser (VCSEL), ultra-high speed communication, wireless power transfer, energy harvesting, 1-bit communication, radio frequency (RF), wideband.

List of Publications

Appended Publications

This thesis is based on work contained in the following papers:

[A] I. C. Sezgin, J. Gustavsson, T. Lengyel, T. Eriksson, Z. S. He, and C. Fager, "Effect of VCSEL characteristics on ultra-high speed sigma-delta-over-fiber communication links," *J. Lightw. Technol.*, vol. 37, no. 9, pp. 2109-2119, 1 May, 2019.

[B] I. C. Sezgin, T. Eriksson, J. Gustavsson, and C. Fager, "A flexible multi-Gbps transmitter using ultra-high speed sigma-delta-over-fiber," in *IEEE MTT-S Int. Microw. Symp. Dig.*, pp. 1195–1198, Jun. 2018.

[C] I. C. Sezgin, M. Dahlgren, T. Eriksson, M. Coldrey, C. Larsson, J. Gustavsson, and C. Fager, "A low-complexity distributed-MIMO testbed based on high-speed sigma-delta-over-fiber," *IEEE Trans. Microw. Theory Techn.*, vol. 67, no. 7, pp. 2861-2872, July 2019.

[D] I. C. Sezgin, T. Eriksson, J. Gustavsson, and C. Fager, "Evaluation of distributed MIMO communication using a low-complexity sigma-delta-over-fiber testbed," *IEEE MTT-S Int. Microw. Symp. Dig.*, pp. 754-757, Jun. 2019.

[E] I. C. Sezgin, J. P. Cisneros, and C. Fager, "Evaluation of Simultaneous Wireless Information and Power Transfer with Distributed Antennas," accepted for a presentation at *EuMA European Microwave Week* , Jan. 2021.

[F] I. C. Sezgin, L. Aabel, S. Jacobsson, G. Durisi, Z. S. He, and C. Fager, "All-Digital, Radio-over-Fiber, Time-Division Duplex Communication Link for Distributed Antenna Systems," submitted to *J. Lightw. Technol.*, Oct. 2020.

Other Publications

The content of the following publications partially overlaps with the appended papers or is out of the scope of this thesis.

[a] I.C. Sezgin, C. Fager, L. Aabel, S. Jacobsson, and M. Coldrey "Radio transceiver device configured for dithering of a received signal," Patent application, PCT/SE2019/050638, Jun. 2019.

[b] S. Jacobsson, L. Aabel, M. Coldrey, I. C. Sezgin, C. Fager, G. Durisi, Christoph Studer "Massive MU-MIMO-OFDM uplink with direct RF-sampling and 1-Bit ADCs," *IEEE Globecom Workshops (GC Wkshps)*, Waikoloa, HI, USA, 2019, pp. 1-6.

[c] L. Aabel, G. Durisi, I. C. Sezgin,S. Jacobsson, C. Fager, M. Coldrey "Distributed massive MIMO via all-digital radio-over-fiber," accepted for presentation at *Fiftieth Asilomar Conference on Signals, Systems and Computers*, 2020.

Thesis

[d] I.C. Sezgin, "Sigma-Delta-over-Fiber for High-Speed Wireless Communication Systems," Licentiate dissertation, Dept. of Microtechnology and Nanoscience, Chalmers University of Technology, Gothenburg, Sweden, Apr. 2019.

As part of the author's doctoral studies, some of the work has previously been published in [d]. Text, figures and tables from [d] may therefore be fully or partially reproduced in this thesis.

Abbreviations

5G	Fifth Generation Mobile Networks
AP	Access Point
ARoF	Analog-Radio-over-Fiber
CFO	Carrier-frequency Offset
CFP	C-form-factor Pluggable Transceiver
CPRI	Common Public Radio Interface
CSI	Channel State Information
CU	Center Unit
DAC	Digital-to-Analog Converter
DSP	Digital Signal Processing
DRoF	Digital-Radio-over-Fiber
EAM	Electro-absorption Modulator
EVM	Error Vector Magnitude
FPGA	Field-programmable Gate Array
HBR	Heat-to-bitrate Ratio
IF	Intermediate Frequency
IMD	Intermodulation Distortion
LNA	Low-noise Amplifier
LO	Local Oscillator
MIMO	Multiple Input Multiple Output
MMF	Multi-mode Fiber
NTF	Noise Transfer Function
OBSAI	Open Base Station Architecture Initiative
OSR	Oversampling Ratio
PA	Power Amplifier
RAM	Random-access-memory
RoF	Radio-over-Fiber
PPG	Pulse-pattern Generator
PWM	Pulse-width Modulation
RF	Radio Frequency
RRH	Remote Radio Head
RU	Remote Unit
SDM	Sigma Delta Modulation
SDoF	Sigma-Delta-over-Fiber

SIR	Signal-to-interference Ratio
SFP	Small Form-factor Pluggable Transceiver
SMF	Single-mode Fiber
SNR	Signal-to-noise Ratio
STF	Signal Transfer Function
VCSEL	Vertical-Cavity Surface-Emitting-Lasers

Contents

Chapter 1

Introduction

Our lives are changing dramatically with the development of communication technology. Almost without any effort, just by using your phone, you can socialize with your friends, let your friends see what you are eating, check your emails, watch an ultra-high-definition (UHD) movie while travelling, pay your bills, surf through the limitless world of the Internet. It has become obsolete to carry a map of the city your are travelling or a dictionary when you are abroad. You need only one thing: your mobile phone with high-speed internet access.

All these charming benefits of mobile internet access attract more and more users. In 2019, 740 million new subscriptions are made to mobile LTE services globally [1]. Today, there are more than 4.29 billion LTE subscriptions, globally, and it is expected that in 2025 the total number of LTE and 5G subscriptions will be 7.18 billion. The average monthly data traffic per subscription is expected to increase from 7 gigabytes (GB) to 25 GB in this time period, corresponding to a total data traffic increase from 33 exabyte (EB) to 164 EB per month [1].

The communication speed has grown exponentially during the evolution of mobile communication technology. The second generation mobile communication technology (2G) was able to transmit 64 kbps in 1990s. In 2004 a maximum data rate of 2 Mbps was available with the third generation mobile system (3G). Today, a mobile phone can communicate at a date rate between 200 Mbps and 1 Gbps thanks to the fourth generation mobile system (4G). The latest mobile system technology 5G, which is currently being deployed, is expected to provide data rates higher than 1 Gbps [2].

These high speed communications and the new life style of *always being connected* are enabled by a wireless communication link between a mobile phone and base-stations (BS). In a nutshell, when a user wants to transmit and/or receive data, his or her mobile phone communicates through an antenna located at an antenna tower, see Fig 1.1. Thereafter, the information received by the antenna is transferred to a base-station central unit (CU) located close to the tower. The communication link between the remote radio head (RRH) and the base-station CU, mobile fronthaul, can be formed either by electrical or optical cables. In 4G-LTE, mobile fronthaul links are commonly formed by radio-over-fiber (RoF) through common public radio interface (CPRI) [3] standard.

The previously mentioned constant demand of higher data rates and increased coverage requires major improvements of these fronthaul links between the antenna and the control unit in a base-station. Many more antenna towers

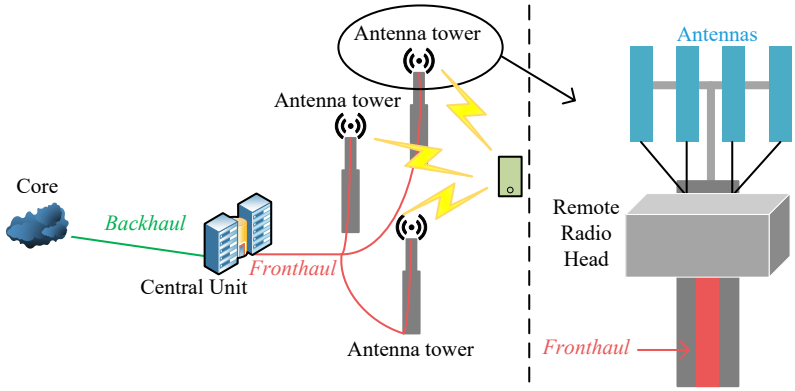

Figure 1.1: A conceptual schematic of mobile network communication systems.

will be deployed in 5G systems, compared to 3G and 4G, in order to fulfill the communication standard requirements, i.e. cell densification [4]. Hence, the RRHs at the antenna towers have to be low-cost, low-size and power efficient [5].

Similar to 4G-LTE, radio-over-fiber solutions are considered for realizing the mobile fronthaul in 5G network systems [5, 6]. Hence, the chapter will continue with introducing the radio-over-fiber technology and its various types.

1.1 Radio-over-Fiber

Utilizing optical fibers to distribute radio communication signals was first proposed in 1990 [7, 8]. Since then, it has been developing rapidly and today it is used in many different areas including: radio signal distribution, electronic warfare, terahertz spectroscopy [9]. The main advantage of RoF, is exploiting the low-loss and wide bandwidth nature of optical communication to distribute high frequency radio signals over a large distance.

The RoF technique simplifies the conventional BSs by shifting the main/complex operations from the radio unit to a CU, which communicates with multiple BSs [10]. In RoF, an electrical radio signal modulates an optical source, thereafter an optical fiber transports the optical signal to a remote unit, where it is converted back to the electrical domain with a photo detector. The optical fiber provides a low attenuation and interference free communication medium. The RoF technique has different variants, each with different advantages and disadvantages. Below, the three most common implementations are discussed.

1.1.1 Analog-Radio-over-Fiber

The traditional implementation of RoF utilizes analog modulation, and is therefore called analog-radio-over-fiber (ARoF) [11–16]. In ARoF, a digital communication signal is transformed to an analog signal by a digital-to-analog converter (DAC), see Fig 1.2 (a). After that, the analog electrical signal drives an optical source, which is followed by an optical fiber. At the far end of the fiber, the electrical signal is recovered with a photo-diode. After that the electrical signal is filtered, amplified and finally transmitted over the air by an

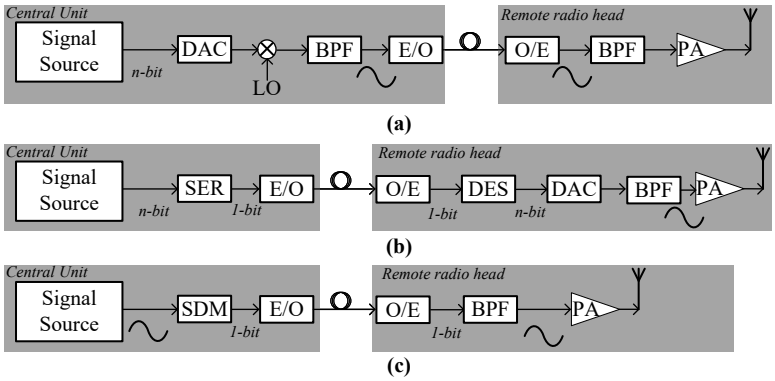

Figure 1.2: General structure of (a) ARoF, (b) DRoF, and (c) SDoF. DAC: Digital to Analog Converter, BPF: Bandpass Filter, E/O: Electrical to Optical Converter, O/E: Optical to Electrical Converter, PA: Power Amplifier, SER: Serializer, DES: Deserializer, SDM: Sigma Delta Modulator.

antenna. The upconversion to the wireless communication frequency can be performed both at the CU or at the RRH. As illustrated in Fig 1.2 (a), the up-conversion stage at the CU simplifies the RRH by eliminating the local-oscillator and mixer stages in it. However, using this method for transmission of up-converted signals requires an optical laser capable of generating high-speed optical signals and a photodetector directly generating the corresponding electrical signal. Designing such components is not an easy task, especially for mmWave communication systems at and beyond 28-GHz frequency. A method to mitigate the chromatic dispersion and the requirement of high-speed optical components is to transmit baseband or intermediate-frequency (IF) signals over the fiber [17]. However, this technique increases the complexity of the RRH due to performing the up-conversion stage at the RRH.

Another main limitation of ARoF is the nonlinearities of the optical components, e.g. laser, photodetector, resulting in inter-modulation distortion (IMD) [18]. In [19] it is shown that these non-linearities are the main performance limitation of ARoF communication links, since it effects the dynamic range of the link. Furthermore, the chromatic dispersion effect of optical fiber is another disadvantage of ARoF, especially for mm-wave communication systems with ultra-wide bandwidth signals [20].

1.1.2 Digital-Radio-over-Fiber

An alternative to ARoF is to transmit digital signals in the optical channel, rather than analog ones. This technique is called digitized-radio-over-fiber (DRoF) [21, 22]. In the DRoF communication scheme, a serialized digital signal is transmitted, see Fig 1.2 (b). The digital signal modulates an optical laser, which is followed by an optical fiber. At the remote unit, the optical signal is converted back to electrical domain and de-serialized. Thereafter, the digital signal is transformed to an analog signal with a high-bandwidth DAC. Finally, the electrical signal is filtered, amplified and transmitted over the air by an antenna.

If the up-conversion stage is performed at the remote unit, the complexity

of it increases. On the other hand, the small fractional bandwidths of most common wireless standards, (e.g. WI-FI, 3G, 4G), relative to their carrier frequencies, enable the use of bandpass sampling techniques [21, 23]. In this way, the sampling rate requirements of the ADC/DAC decreases drastically, since bandpass sampling enables to sample a signal with a frequency much lower than its Nyquist rate. Bandpass sampling technique requires the ADC to be able to operate at the highest frequency component of the upconverted RF signal with a sampling rate equal or higher than two times the information bandwidth. This is very challenging for mmWave systems due to very high frequency components of the communication signals [24]. Overall, the digital signal transmission eliminates the non-linearity and dynamic range limitation of ARoF [25] at the cost of employing ADCs and DACs at the remote unit.

It is worth to mention that, DRoF is a standardized communication method for cellular networks, e.g. open base station architecture initiative (OBSAI) [26] and common public radio interface (CPRI) [3], which utilizes baseband signal transmission through the fiber and an upconversion stage at the RRH.

1.1.3 Sigma-Delta-over-Fiber

Another technique to realize RoF links is sigma-delta-over-fiber (SDoF). It was first proposed [27] as an alternative RoF technique offering advantages of both ARoF and DRoF. Similar to DRoF, it utilizes a digital-optical link between the central and remote unit, see Fig. 1.2 (c). Hence, it has the previously mentioned benefits of DRoF in terms of non-linearity and dynamic range. Moreover, the sigma-delta modulator eliminates the DAC from the remote unit, since the analog signal can be recovered only with a bandpass filter. The digital up-conversion stage at the CU provides a very low-complexity remote unit.

1.2 Thesis Contributions and Outline

In this thesis, the potential and limitations of sigma-delta-over-fiber communication links are investigated. Chapter 2, starts with an introduction to sigma-delta modulation, followed by various implementation types. The advantages and limitations of different variants of SDoF communication schemes, depending on the band of operation, are also presented.

The need for larger bandwidths necessitates to use higher carrier frequencies than today. This results in increased number of central-stations and remote radio units. Forming the links between the central stations and remote units by SDoF is a promising method to keep the cost and complexity low. An ultra-high-speed SDoF communication link is realized with state-of-the-art vertical-cavity surface-emitting-lasers (VCSEL) in order to evaluate its maximum performance and applicability. VCSELs provide many benefits, such as low power consumption, high-bandwidth density, low manufacturing and packaging costs, hence they are very strong candidates as an optical source for ultra-high-speed SDoF communication links. In Chapter 2, the performance and power consumption of such links are investigated with different VCSELs and various signals. The effects of the laser characteristics are evaluated by various experiments [Paper A]. The potential and limitations of SDoF at carrier

frequencies beyond 10 GHz for transmission of wideband modulated signals are also investigated [Paper B].

MIMO is one of the key technologies behind the current (4G) and future generation (5G and beyond) mobile communication networks. Physically distributing the antenna elements/access points of a MIMO system is a method to further increase the capacity and the coverage. However, the phase synchronization requirement of such distributed MIMO (D-MIMO) communication techniques requires extra measures due to the large distance between the access points. The existing D-MIMO implementations are designed for real-time communication and they are costly and complicated when it comes to the experimental studies. Hence, there is also a need for low-cost, low-complexity platforms aimed for initial and fundamental D-MIMO studies and experiments at an early stage. In Chapter 3, this problem is addressed and a novel method to form distributed MIMO communication systems is proposed by employing sigma-delta-over-fiber. The proposed testbed in [Paper C], employs an all-digital sigma-delta-over-fiber architecture to generate and distribute RF communication signals from a single central station to multiple spatially distributed remote units, using an FPGA and standard high-speed digital optical interconnect components. The centralized structure provides excellent phase coherency between physically distributed remote units. Furthermore, it decreases the complexity and cost of the remote units significantly, while enabling a highly flexible testbed due to the all-digital structure. The testbed is evaluated in terms of RF-phase coherency and flexibility (symbolrate and carrier frequency) [Paper C],[Paper F]. Furthermore, various wireless communication experiments are performed with the proposed testbed and the results are presented in [Paper D]. Finally, the testbed is used to demonstrate simultaneous wireless information and power transfer (SWIPT) with distributed antennas [Paper E].

SDoF offers many benefits when employed to realize the downlink, from CU to antenna elements, of a wireless communication system. However, a suitable uplink is difficult to obtain without compromising the low cost, low complexity RRHs of the system. More conventional RoF techniques such as ARoF and DRoF could be implemented, but they would significantly increase the complexity and cost of the communication system, which eliminates many benefits of SDoF. Therefore, there is a need for a corresponding low-complexity, all-digital communication link to be employed in SDoF systems. Essentially, a method to directly encode the received RF signal from the user equipment to a binary stream is desired at the RRH. It is desirable that, this operation should be performed without any extra frequency conversion or time domain sampling, since these should be performed at the CU of the communication system. In Chapter 4, an uplink architecture fulfilling all above mentioned requirements is proposed [Paper F]. The architecture is carefully investigated through simulations and measurements with different signals.

Overall, this thesis addresses cost, complexity, flexibility, scalability requirements of emerging and future wireless communication systems by proposing sigma-delta-over-fiber solutions.

Chapter 2

Sigma-Delta-over-Fiber

Sigma-delta-over-fiber is a variant of radio-over-fiber, which employs sigma-delta modulation (SDM) in order to generate and transmit digital signals with few discrete amplitude levels through optical fiber. The key aspect of SDoF communication is encoding the upconverted RF-signal into a low-resolution digital signal and transmitting it through an optical fiber. Similar to DRoF, digital signal transmission is highly resilient to non-linearities [27]. In contrast, the power-hungry, high-bandwidth DAC of DRoF is not needed at the remote unit, since the communication signal is recovered only by a band-pass filter [28]. This results in a much simplified remote unit, similar to ARoF. Overall, SDoF provides the linearity of DRoF communication link, while maintaining low-cost and low-complexity remote units similar to ARoF.

It is worth to mention that, SDoF is enabled by the fact that digital signal processing (DSP) units and serial clock rates have increased quickly and now are into the microwave regime. Without these developments, it would not be possible to consider SDoF for RF communication. Furthermore, SDoF can benefit from the demands for low-cost, high capacity interconnects in data centers, which is driving the development of binary transceivers and optical interconnects with higher and higher clock rates. (SDoF benefits from these developments, since it employs binary, digital communication links.)

2.1 System Overview

In Fig. 2.1, a general block diagram of a two-level, radio-frequency sigma-delta-over-fiber (RF-SDoF) downlink is presented [27, 28]. As illustrated there, RF-SDoF systems consist of three main blocks: a CU, an optical communication link, and a remote unit. Starting at the CU, a binary signal carrying the upconverted RF-signal is generated. Then, the binary signal is converted to optical domain with an optical source, typically a laser. At the far end of the optical fiber, the electrical signal is recovered with a photo detector. Thereafter, the quantization noise of SDM is suppressed by a band-pass filter to recover the upconverted, analog RF-signal, before the RF amplification, see Fig. 2.1. Finally, the analog signal is amplified and transmitted by an antenna. The following sections will present the main blocks of a SDoF system and thereafter various implementation examples will be discussed.

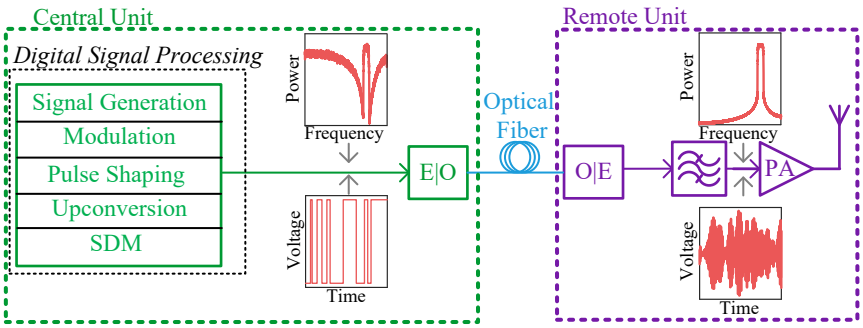

Figure 2.1: General structure of band-pass sigma-delta-over-fiber link including the spectra and waveforms. The recovered signal after the bandpass filter is also presented.

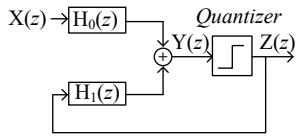

Figure 2.2: A z-domain model of sigma-delta modulation.

2.2 Central Unit

The CU is the first block of a SDoF link, in which the digital signal processing and electrical to optical domain conversion is performed, see Fig. 2.1. The fundamental difference of the SDoF digital signal processing block compared to other RoF techniques, is the use of sigma-delta modulation to generate binary signals. Hence, this section starts with introducing the SDM, which is followed by a section about the electrical to optical conversion.

2.2.1 Sigma-Delta Modulation

Sigma-delta modulation is a technique where a waveform is quantized to a very low resolution signal with the help of oversampling and noise shaping. The quantization produces large, wideband noise-like distortion, referred as quantization noise. By oversampling, the quantization noise is spread over the frequency spectrum and by noise shaping, the quantization noise is shaped such that it is minimized in the band-of-interest. Overall, a very-high signal-to-noise-ratio (SNR) can be achieved at the band-of-interest [29]. The in-band quantization noise is determined by the order of the SDM and the oversampling ratio (OSR) [29]. OSR is defined as the ratio of SDM sampling rate to Nyquist rate of the signal:

$$\mathrm{OSR} = \frac{f_s}{2\mathrm{BW}}, \tag{2.1}$$

where BW represents the bandwidth of the modulated RF signal.

A sigma-delta modulator can be modelled as shown in Fig. 2.2. The output of the loop-filter in (z)-domain is:

$$\mathrm{Y}(z) = \mathrm{H}_0(z)\mathrm{X}(z) + \mathrm{H}_1(z)\mathrm{Z}(z). \tag{2.2}$$

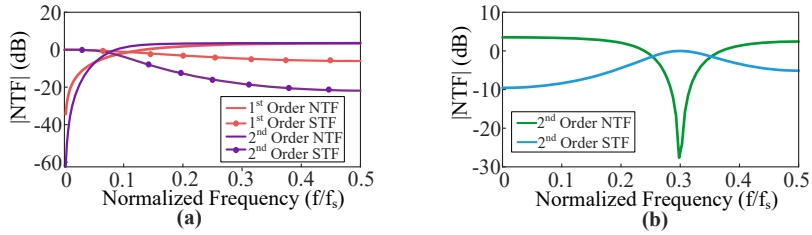

Figure 2.3: (a) Signal and noise transfer function magnitude of first and second order low-pass sigma-delta modulation. (b) Signal and noise transfer function magnitude of second order band-pass sigma-delta modulation.

The quantization can be represented as an additive error signal source [30]. The output of the modulator becomes:

$$\mathrm{Z}(z) = \mathrm{Y}(z) + \mathrm{E}(z), \tag{2.3}$$

where $\mathrm{E}(z)$ represents the white quantization noise, i.e. the error signal. Using these two equations the output of the quantizer, $\mathrm{Z}(z)$, can be re-written as:

$$\mathrm{Z}(z) = \frac{\mathrm{H}_0(z)}{1 - \mathrm{H}_1(z)}\mathrm{X}(z) + \frac{1}{1 - \mathrm{H}_1(z)}\mathrm{E}(z). \tag{2.4}$$

The transfer function of the modulator when the quantizer noise is neglected is denoted as signal transfer function (STF) and is equal to:

$$\mathrm{STF}(z) = \frac{\mathrm{H}_0(z)}{1 - \mathrm{H}_1(z)}. \tag{2.5}$$

Similarly, the transfer function when the input is neglected, the noise transfer function (NTF), is:

$$\mathrm{NTF}(z) = \frac{1}{1 - \mathrm{H}_1(z)}. \tag{2.6}$$

Equation (2.6) suggests that, in order to minimize the quantization noise at a certain frequency range, $\mathrm{H}_1(z)$ must be large at that frequency range. Furthermore, $\mathrm{H}_0(z)$ must also be large at the same frequency in order to have a STF that is close to or larger than unity, see (2.5). The SD-modulator operating principle can be represented by the STF and the NTF. Only by choosing appropriate loop filter transfer functions, $\mathrm{H}_0(z)$ and $\mathrm{H}_1(z)$, the quantization noise can be minimized at and around any frequency, while preserving the input signal quality. In this way, a high SNR will be achieved at the band of interest.

NTF and STF of first and second order low-pass and second order band-pass SDM are presented in Fig. 2.3 (a) and Fig. 2.3 (b), respectively. The minimized quantization noise and the unity STF at the band-of-interest is clearly visible. As mentioned previously, the in-band quantization noise can be decreased by increasing the order of the SDM. This is also illustrated in the same figure. However, higher order SDM can result in unstable SDMs. Stability of a SDM depends on the maximum out of band gain, which is determined by the $\mathrm{NTF}(z)$ and the input signal magnitude range. There are no proven methods to assure the stability of SDMs. The most common criterion is given by Lee's Rule [31,32].

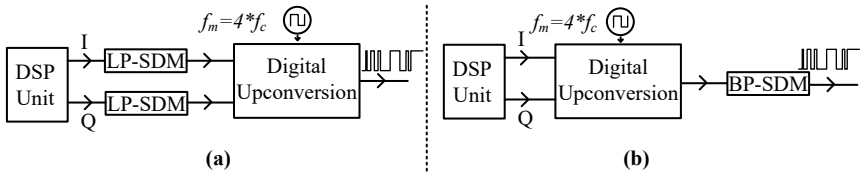

Figure 2.4: Block diagrams of two different RF sigma-delta-over-fiber structures, (a) using lowpass sigma-delta modulation, (b) using bandpass sigma-delta modulation. Both implementations transfer upconverted RF-signals encoded to binary streams over the fiber.

According to that rule, a SDM is likely to be stable if the maximum gain of NTF(z) over all frequencies is smaller than 1.5. However, this is more like a guide than a proven rule, since it does not consider the input range and there are some examples of stable SDM with a maximum gain larger than 1.5 [29].

2.2.2 Optical Source

After the sigma-delta modulation, the digital signal is transmitted to an optical source with a binary transmitter, e.g. FPGA. The electrical to optical conversion can be performed with many different types of lasers and optical modulators: single-mode laser diode [33], Mach-Zender modulator [34], VCSEL [35], electro-absorption modulator (EAM) [36]. Moreover, two-level SDoF communication links can also utilize standardized optical interconnects [37, 38]. Different types of small form-factor pluggable (SFP, SFP+, XFP, QSFP, QSFP+, QSFP28) and C-form-factor pluggable (CFP) transceivers are some of the most common ones.

2.3 Optical Fiber and Remote Unit

The central and remote units are connected to each other with an optical fiber, see Fig. 2.1. The optical fiber selection depends on the link distance. In general, single-mode-fibers are employed in SDoF communication links longer than few kilometers, for example, 25 km [39], 80 km [40] , whereas multi-mode-fibers are more common in shorter distances, 200 m [28].

The remote unit is responsible for electrical signal recovery, i.e. optical to electrical conversion through a photo-diode [33], filtering the out-of band quantization noise, amplification of the signal and finally the transmission of the signal by an antenna. A local-oscillator and mixer stage might me employed depending on the implementation of the system.

2.3.1 Implementation Examples

RF-SDoF can be implemented by a lowpass SDM (LPSDM) or a bandpass SDM (BPSDM), see Fig. 2.4. In general, low-pass sigma-delta-modulators (LPSDM) are employed in RF-SDoF systems due to lower sampling requirements at the CU processor. In such structure, the SDM operates on the oversampled baseband I and Q signals. After the SDM, the two, one-bit streams are digitaly upconverted to their carrier frequencies. The up-conversion is typically performed by a 4×1 multiplexer operating at $f_m = 4f_c$, since it greatly

simplifies the operation [41]. The low-pass sigma-delta modulated I, Q and their negative copies -I, -Q are transmitted in the presented order resulting in a carrier frequency $f_c = f_m/4$, as illustrated in Fig. 2.4.

There are various RF-SDoF implementations employing LPSDM. In [42], it is shown that, with the current state-of-the-art technology, up to 100 GSa/s SDMs can be operated real-time which provides 25 GHz carrier frequency with a net information bitrate of 3.125 Gb/s. In [38], a real time SDoF MIMO system with four transmitter antennas using 3.5 GHz carrier frequency is demonstrated. [43] presents a real-time SDoF distributed antenna system suitable for 5G fronthaul downlink at the frequency range 1 (410 MHz–7.125 GHz). One of the earlier studies [37], employs LPSDM and demonstrates a RF-SDoF with 920 MHz carrier frequency.

Another approach is to perform the the digital upconversion before the bandpass SDM (BPSDM), see Fig. 2.4 (b). In [44] and [45] such an implementation is demonstrated with both 4G-LTE and 5G-NR signal at a carrier frequency of 960-MHz.

All of the above mentioned systems transmit signals at their RF carrier frequencies from the CU, i.e. form RF-SDoF systems. However, it is also possible to transmit intermediate frequency (IF) signals and perform the upconversion at the RRH without sacrificing the RF-phase coherency for 5G frequency range 2 (above 24 GHz). In [46], signals at 2.4 GHz center frequency are transmitted through the optical link to two seperate RRHs. At each RRH, a clock and data recovery (CDR) circuit is utilized to generate a clock for the upconversion to 25-GHz. In this way, RF-phase coherency is maintained between physically separated RRHs.

Sigma-delta modulators are employed in many different applications in addition to radio-over-fiber communication systems. For example, in power amplifiers [47, 48], visible light communications [49, 50], digital receivers [51, 52] and digital transmitters. When it comes to the digital transmitters, generally, low-pass SDMs [53–60] are preferred together with the aforementioned multiplexer based digital upconversion stage due to lowered sampling rate requirements compared to band-pass SDMs. There are also demonstrations of multi-band [61–63] SDMs. In such implementations, the quantization noise is minimized in two different bands in the first Nyquist zone. These modulators are highly useful in digital transmitters with simultaneous multi-band operations. Furthermore, in [39, 40] SDMs are used as a digitization method for mobile fronthaul network by replacing the ADCs of the CPRI standard.

In [33], a LP-SDM signal centered at 10 MHz is transmitted to the remote unit. The signal is first band-pass filtered to attenuate the quantization noise, then it is upconverted by a conventional analog mixer and local-oscillator stage. Compared to the previous digital-up conversion systems, the carrier frequency selection is less-limited. However, this method suffers from increased remote unit complexity compared to all the other mentioned methods. Furthermore, a method to maintain RF-phase coherency between multiple RRHs is not suggested.

A more unorthodox method is presented in [34] to employ a carrier frequency of $f_c = 60$ GHz. The low-pass sigma-delta modulated I-Q signal is first upconverted to 3.2 GHz by a multiplexer operating at 12.8 Gbps, as mentioned previously. Then, by using optical heterodyning, the carrier frequency is shifted

to 60 GHz in optical domain. Such implementation facilitates the generation of mmWave carrier frequencies without extremely high SDM sampling rates.

As discussed in this section there are various types of SDoF implementations with different SDMs, carrier frequencies, band-of-operations, etc. Each of them has different benefits and limitations in terms of the system complexity, flexibility, and cost. In the following section, an ultra-high-speed implementation example will be presented and evaluated under different signals.

2.4 Ultra-High-Speed Implementation and Effects of the VCSELs

In this section, an ultra-high-speed RF-SDoF communication link is established as an example and evaluated with beyond-10 GHz signals using state-of-the-art VCSELs. First, the effects of VCSEL characteristics on ultra-high-speed SDoF communication links are examined [Paper A]. Thereafter, the potentials and limitations in terms of the data-rate and carrier frequency are investigated [Paper B].

2.4.1 Vertical-Cavity Surface-Emitting-Laser

The VCSEL is a semiconductor laser diode, which was proposed in 1977 by Professor K.Iga at Tokyo Institute of Technology [64]. Compared to conventional edge-emitting lasers, VCSELs have a light output perpendicular to its surface, see Fig. 2.5 (a). Even though VCSELs are mostly utilized in datacom centers as optical sources, they are also used in many other applications from sensing to communication. Atomic clocks [65], laser printers [66], face identification in Apple devices [67], gas analysis [68] and optical computer mouse [69] are some of these applications.

The low manufacturing and packaging costs enabled by wafer-scale testing and screening are some of the major benefits of VCSELs [70]. Moreover, the use of plastic coupling optics and large alignment tolerance to multi-mode-fibers (MMF) has made VCSELs even more popular. VCSELs also provide small footprint required for low power consumption and high bandwidth density. Overall, these properties make VCSELs very good candidates as optical sources for ultra-high speed SDoF communication links.

Operational Considerations

One important fact to consider when using VCSELs, is avoiding subthreshold 0-state. In other words, turning-off the laser when '0' signal is transmitted. This is mainly due to the unwanted consequences of subthreshold 0-state, such as turn-on delay and power overshoot. The consequences of both are explained further in the following subsection. In Fig. 2.5 (b), three different modulation conditions are illustrated. The red curve represents the case where subthreshold 0-state is avoided by using a certain modulation amplitude and bias current. In the case represented by the green curve, the same modulation amplitude is used with a lower bias current, resulting in a subthreshold 0-state operation. The blue curve represents the case where the bias current is same as the operation

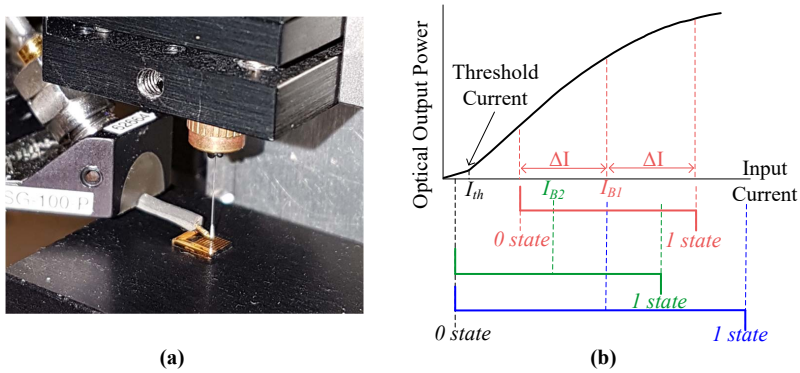

Figure 2.5: (a) A chip with multiple VCSELs on it and one of the VCSELs coupled directly to optical fiber.(b) Illustration of three different modulation conditions for a VCSEL. I_{th} and I_{B} represents the threshold and bias current, respectively. The first condition (red curve) has bias current I_{B1} and both states are above threshold. The second condition (green curve) has the same modulation amplitude as the first condition but a smaller bias current, I_{B2}, resulting in subthreshold 0-state. The third condition (blue curve) has the same bias current with the first condition, I_{B1}, however with a larger modulation modulation amplitude then the first condition, which yields to subthreshold 0-state.

represented by the red curve, however with a higher modulation amplitude, again resulting in a subthreshold 0-state. These three cases illustrate that, to avoid subthreshold 0-state operation, both the modulation amplitude and the bias current has to be chosen carefully.

Furthermore, choosing a correct bias current and input modulation amplitude is not only important for avoiding the subthreshold 0-state, but also important for energy efficiency, lifespan, bandwidth (determined by the bias current), etc. For example, larger modulation amplitudes require higher bias currents in order to avoid threshold effects, which results in low energy efficiency and low potential lifespan of the VCSEL. All of these mentioned properties are highly affected by the VCSEL oxide aperture size as well.

These effects of the VCSEL characteristics and operating points are less-known for SDoF communication links, especially for beyond-10 GHz systems. The following subsections demonstrate the trade-offs between VCSEL characteristics, operating points, and oxide aperture sizes.

2.4.2 Experimented VCSELs

For the evaluation experiments, the ultra-high-speed SDoF communication links are formed by three 850 nm state-of-the-art VCSELs. These VCSELs are GaAs-based and the design procedures are described in detail in [71]. The procedure that is explained in [71], enabled a 8 μm VCSEL to achieve a record high OOK data transmission rate of 55 Gbps over 50m of OM4-fiber without equalization electronics [72]. All the experiments are performed with VCSELs that are manufactured in Chalmers University of Technology with the same technology.

Fig. 2.6 shows the steady-state characteristics of the three VCSELs at room temperature. The left and right graphs present (a) the optical output power

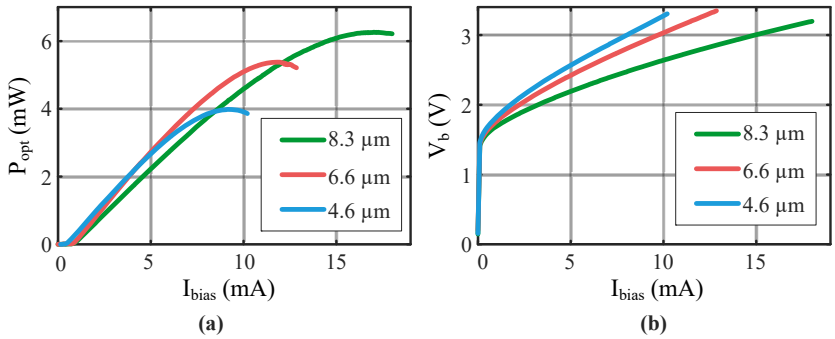

Figure 2.6: DC characteristics of each VCSEL. (a) Optical output power and (b) voltage drop with respect to bias current.

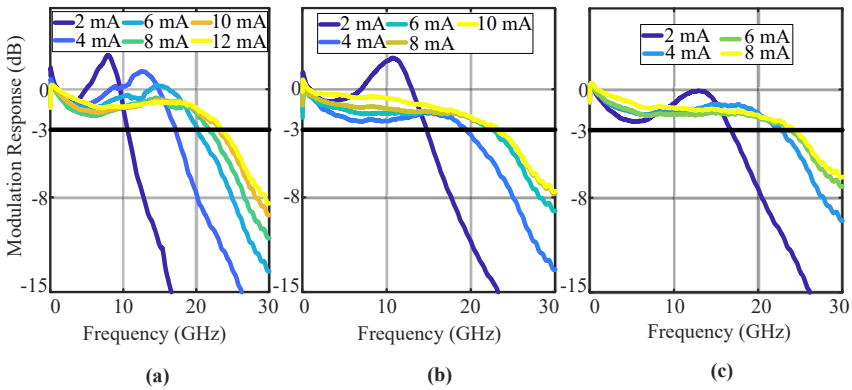

Figure 2.7: Small-signal modulation response (S21) for VCSELs with oxide aperture sizes of (a) 8.3 μm, (b) 6.6 μm and (c) 4.6 μm with respect to bias current. The modulation response is normalized by dividing with its value at 1 GHz. 3-dB bandwidth of the VCSELs are also shown (black line) for each VCSEL.

and (b) the voltage drop with respect to bias current, respectively. When the three VCSELs are compared, VCSELs with larger oxide apertures have higher maximum output power, larger threshold current and a lower differential resistance.

Small-signal modulation response of each VCSEL is shown in Fig. 2.7. The highest 3-dB bandwidth of each VCSEL for the presented bias currents are ~24.5 GHz (at I_{bias}=8mA), 23.5 GHz (at I_{bias}=10mA) and 23.5 GHz (at I_{bias}=12mA) for the VCSELs with oxide aperture size of 4.6 μm, 6.6 μm and 8.3 μm, respectively.

2.4.3 Effects of VCSEL Characteristics

Optical interconnects based on directly modulated VCSELs and multi-mode-fibers (MMF) are today widely used in datacom applications [73]. Hence, the effects of VCSEL characteristics on optical datacom links are well-known. On the other hand, the effects are less-known for SDoF communication links.

One of the earlier SDoF studies [27], investigated the effects of VCSEL bias

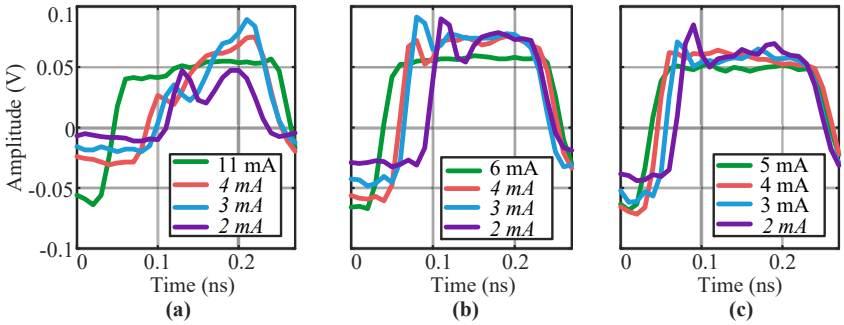

Figure 2.8: Time domain pulse response measured at the electrical output of the photoreceiver as a function of VCSEL bias current for the three employed VCSELs with oxide aperture sizes of (a) 8.3 μm, (b) 6.6 μm, (c) 4.6 μm. 1 V peak-to-peak modulation amplitude is used. The italic written bias currents represents subthreshold 0-state.

current and modulation amplitude on signal quality by employing a 1550-nm VCSEL as an optical source. However, the investigations were performed for signals with carrier frequencies up to 2.25 GHz. In [Paper C], the investigation is extended to carrier frequencies beyond-10 GHz. In addition, VCSELs with different oxide aperture sizes are evaluated. Three, state-of-the-art, 850-nm-wavelength VCSELs with oxide aperture sizes of 8.3, 6.6 and 4.6 μm are employed. Furthermore, various bias currents and input modulation voltages are also tested in order to discover the trade-offs between aperture size, bias current, modulation voltage and signal quality, energy efficiency, lifespan.

During the experiments, a 64-QAM, 160 Msym/s RF-signal centered at 12 GHz and modulated by a 32 Gbps bandpass SDM (OSR = 100) is used as a reference signal.

Turn-on Delay and Power Overshoot

As mentioned previously, subthreshold 0-state leads to signal quality degradation due to power overshoot and turn-on delay. When the electrical input of the VCSEL suddenly changes to switch from 0-state to the 1-state (or vice versa), the optical output will reach its new state undergoing damped relaxation oscillations [74]. This can result in power over- and under-shooting in the transient part of the output response. Furthermore, when the input current changes suddenly from 0- to 1-state, it takes a certain time for the laser to react, i.e. start lasing, which is called turn-on delay. The power overshoot and turn-on delay becomes more pronounced when the 0-state is below or close to the threshold, resulting in significant pulse distortion. To avoid such effects higher bias currents should be used, which leads to lower energy efficiency. Thus, there is a trade-off between pulse distortion and energy efficiency for the VCSELs.

Pulse Distortion

To investigate the effects of turn-on delay and power overshoot on ultra-high-speed SDoF communication links, three studied VCSELs are operated at different bias currents with a constant input modulation amplitude V_{pp}=1 V.

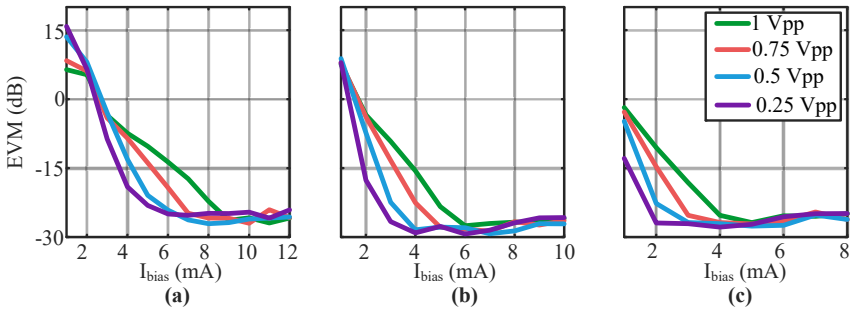

Figure 2.9: Calculated EVM values of the captured symbols for the three employed VCSELs with oxide aperture sizes of (a) 8.3 μm, (b) 6.6 μm, (c) 4.6 μm.

The measured digital pulse responses after the photo-receiver is presented in Fig. 2.8. As expected, the impact of the turn-on delay and power overshoot is highest for the lowest bias current (green curves) since the 0-state is lowered with a lower bias current. The turn-on delay and power overshoot decreases and eventually disappears when the bias current is increased, which is due to the increasing level of the 0-state. Moreover, same bias currents result in different 0-state levels for different VCSELs. For example, when the 4.6 μm VCSEL is biased at 3 mA the 0-state is above the threshold, whereas for the 6.6 μm VCSEL same current results in subthreshold 0-state. The reason for this is the fact that the current swing of the larger aperture VCSEL is much higher than the smaller VCSEL, for the same voltage swing. The curves representing the highest bias currents (yellow curves) in Fig. 2.8 do not show any power overshoot or turn-on delay, indicating a well-over threshold 0-state operation. Hence, the effect of pulse distortion is significantly decreased on SDoF communication link.

Effect on the Link Performance

The level of 0-state is not only dependent on the bias current but also the input modulation amplitude. To discover and quantify the effect of turn-on delay and power overshoot on SDoF-link performance, experiments with all three VCSELs are performed with different bias currents and input amplitudes. The calculated EVM of the captured symbols are presented in Fig. 2.9. The SDoF-link performance increases significantly for higher bias currents and lower input amplitudes, regardless of the employed VCSEL. This is an expected consequence of 0-state level being further away from the threshold, decreasing the pulse distortion caused by power overshoot and turn-on delay. Another important observation is that each VCSEL achieves similar performance at the optimum operating point, which is limited by the noise floor of the PPG . Moreover, for a given bias current and modulation amplitude, smaller VCSELs exhibit less power overshoot and turn-on delay, see Fig. 2.9. The main reason for this is the fact that smaller volume of the laser results in a higher photon density inside the laser and therefore a higher damping of the relaxation oscillations and lower threshold current [71].

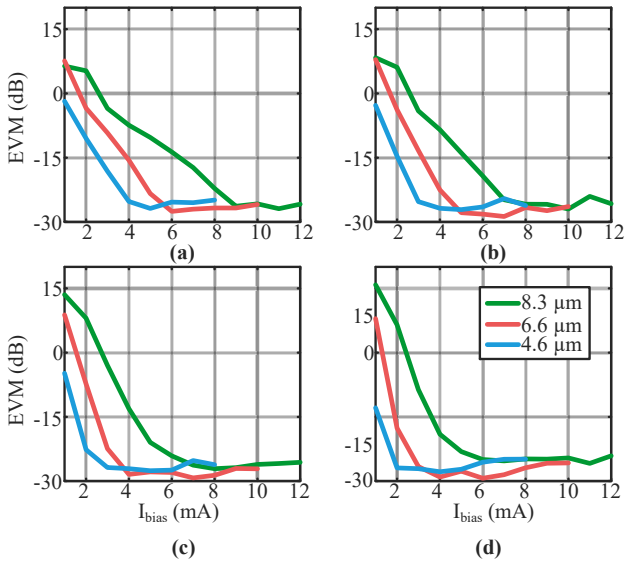

Figure 2.10: Calculated EVM values of the captured symbols for the three employed VCSELs with oxide aperture sizes of 8.3 μm, 6.6 μm, 4.6 μm with respect to bias current and peak-to-peak modulation voltages of (a) 1 V, (b) 0.75 V, (c) 0.5 V and (d) 0.25 V.

Sigma-Delta Stream Error Rate

Bit-error-rate (BER) is an important figure-of-merit of optical datacom communication links formed by VCSELs and MMFs. Typically, datacom links have a requirement of BER $< 2 \times 10^{-4}$ with forward-error correction (FEC). However, the vast oversampling of the RF communication signal in a SDoF-link enables having much higher BER than the typical requirements. For all three VCSELs, the calculated sigma-delta bit-stream error rate (SD-BER) with respect to bias current is presented in Fig. 2.11 (a). The SD-BER is calculated by numerically quantizing the received sigma-delta modulated signal in two levels (in MATLAB) and comparing it to the reference two-level signal. In the figure, black lines represent the minimum bias current required for above-threshold 0-state. As expected, the SD-BER decreases when the bias current is increased, which is due to the decreasing turn-on delay and power overshoot.

In order to examine the effect of SD-BER on the symbol EVM, an ideal SDoF communication link is simulated by injecting random bit-errors. The simulated EVM with respect to SD-BER is presented in Fig. 2.11 (b). According to the simulation results, the measured highest SD-BER (3.3×10^{-3}) should result in a symbol EVM of -31 dB, although in reality it is -28 dB. This shows that the SD-BER is not the limitation of the communication link. Another important result of the simulations is that, even with 10^{-3} SD-BER, much higher error rate than typical datacom requirements, a -35 dB symbol EVM can be achieved. This is one of the major differences between SDoF-links and conventional datacom-links. The eased BER requirements in the SDoF-link makes it possible to use lower VCSEL drive currents, which benefits the VCSEL power consumption and lifetime as discussed in the following subsection.

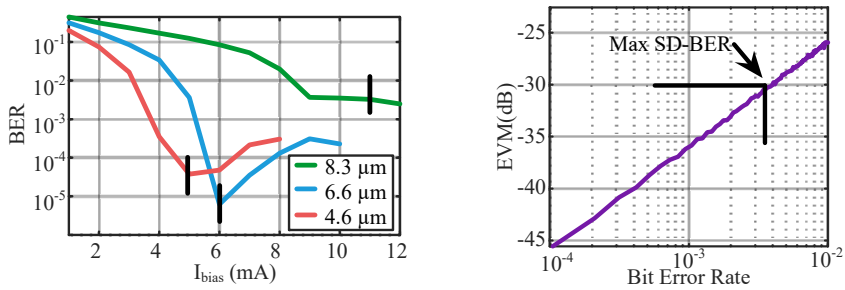

Figure 2.11: (a) Measured sigma-delta stream error rate (SD-BER) for three different VCSELs with respect to bias current for a peak-to-peak input modulation voltage of 1 V. The black lines represent the minimum bias current for above threshold 0-state operation. (b) The simulated symbol EVM with respect to sigma-delta stream error rate. Different numbers of bit errors are injected to the two-level output of the sigma-delta modulator and processed in digital signal processing block of the receiver in MATLAB. The EVM of the demodulated symbols are calculated. The black line represents the highest measured sigma-delta stream rate error, 3.3×10^{-3} and its corresponding EVM of -31 dB. The measured EVM for SD-BER $= 3.3 \times 10^{-3}$ is -28 dB and shows that the communication link is not limited by SD-BER.

Energy Efficiency and Lifetime

Until so far in this chapter, it is shown that each VCSEL can achieve similar performance with proper choice of bias current and input amplitude, see Fig. 2.9. Besides the performance of the communication link, the life span and the energy efficiency are also important properties. Energy efficiency and life span of the VCSEL have an important role in this aspect [75], in datacom applications.

In general, energy efficiency of a VCSEL can be calculated in three different ways: electrical energy-to-data-ratio (EDR), dissipated heat-to-bit rate ratio (HBR), and energy to data distance ratio (EDDR) [76]. In this work we studied HBR, defined by:

$$\mathrm{HBR} = \frac{P_{\mathrm{diss}}}{\mathrm{BR}}, \tag{2.7}$$

where P_{diss} is the dissipated power and BR is the bit-rate. The dissipated power is computed by:

$$P_{\mathrm{diss}} = P_{\mathrm{el}} - P_{\mathrm{opt}} \approx V_{\mathrm{b}} \times I_{\mathrm{b}} - P_{\mathrm{opt,average}}, \tag{2.8}$$

where P_{el} and P_{opt} are the electrical power delivered to, and the optical output power from, the VCSEL, respectively. I_{b}, V_{b} and $P_{\mathrm{opt,average}}$ represent the VCSEL bias current, bias voltage and average optical output power, respectively.

HBR for different bias currents for each VCSEL is presented in Fig. 2.12. As shown previously in Fig. 2.7 (b), smaller VCSELs have higher differential resistance and thereby higher voltage drop at higher bias currents compared to larger VCSELs. Consequently, smaller VCSELs become less efficient at larger bias currents, i.e. higher HBR. On the other hand, to reach a certain EVM performance at the SDoF communication link, smaller VCSELs require smaller bias currents and therefore result in higher energy efficiency.

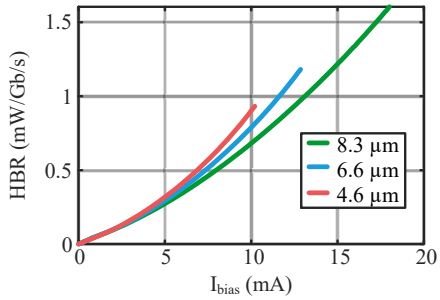

Figure 2.12: Heat-to-bitrate-ratio at 32 Gbps with respect to bias current for each VCSEL.

Lifetime

In cost sensitive applications, the lifetime of VCSELs plays a very important role in order to keep the maintenance cost as low as possible. Typically, the lifetime of a VCSEL is required to be longer than 10 years in such systems, which requires a maximum current density of of $J_{\max} = 10$ kA/cm^2. The maximum current density inside the VCSEL is usually estimated via:

$$J_{\max} = \frac{I_{\text{bias}}}{A_{\text{ox}}}, \tag{2.9}$$

where A_{ox} is the area of the oxide aperture. For the same bias current, smaller VCSELs result in higher $J_{\max}$ hence shorter life span. However, as mentioned previously, smaller VCSELs provide better performance at lower currents due to the eased BER requirements of SDoF and lower pulse distortion caused by the turn-on delay and power overshoot. All the performance trade-offs are summarized in Table 2.1, where the the current density and HBR at the bias current required to reach the minimum EVM (-28 dB) is presented for each of the VCSEL. As shown in the table, the VCSEL having the smallest oxide aperture sizes of 4.6 μm, operating at 2 mA bias current and 0.25 V modulation voltage, can provide minimum EVM at a HBR of only 0.1 mW/Gb/s, while not exceeding a current density of 10 kA/cm^2. Thus, our results indicate that a high performance and energy efficient SDoF-link can be achieved, with long potential lifespan.

2.4.4 Flexibility

After investigating the effects of VCSEL characteristics on SDoF communication link, the potential and the limitations of such links are explored in terms of the central frequency and the data rate.

Carrier Frequency

As mentioned in the previous chapter, SDoF systems benefit from flexible carrier frequencies enabled by the digital up-conversion stage. In this subsection, the performance of an ultra-high speed SDoF communication link is investigated for different carrier frequencies. Signals centered at various carrier frequencies with 32 Gbps sigma-delta sampling rate, 250 Msym/s symbol rate

Table 2.1: Minimum bias current (Bias Cur.) for minimum EVM performance, i.e. EVM ∼-28 dB for different modulation voltages and different VCSELs. For the given bias currents, maximum current density (Current Dens.) (kA/cm^2) inside the VCSELs and the heat-to-bitrate ratio (HBR) (mW/Gb/s) is also presented.

		Aperture Size		
Modulation Voltage		4.6 μm	6.6 μm	4.6 μm
0.25 V_{pp}	Bias Cur.	2	4	6
	Current Dens.	9.45	10.09	8.71
	HBR	0.10	0.22	0.34
0.5 V_{pp}	Bias Cur.	3	4	7
	Current Dens.	14.21	10.09	10.14
	HBR	0.16	0.22	0.42
0.75 V_{pp}	Bias Cur.	4	5	8
	Current Dens.	18.90	12.60	11.61
	HBR	0.23	0.29	0.50
1 V_{pp}	Bias Cur.	5	6	9
	Current Dens.	23.62	15.12	13.06
	HBR	0.27	0.38	0.59

and 64 QAM modulation are transmitted from a pulse-pattern-generator (PPG) (Anritsu MU183020A) and acquired by a high bandwidth oscilloscope (Tektronix DPO733304D). The calculated EVMs of demodulated symbols (Opt.) for different carrier frequencies are presented in Fig. 2.13 (a). Theoretically, the in-band quantization noise power is independent of the carrier frequency [29]. In other words, any carrier frequency in the first Nyquist zone should result very similar signal quality levels. The degraded performance for higher frequencies, despite the theory, is due to the decreasing output power of the PPG (Pow.) and not caused by the SDoF components. This is further verified by acquiring the output of the PPG (El.) without the optical communication link, see Fig. 2.13 (a). The small EVM degradation observed at the optical link is caused by the relative-intensity-noise from the VCSEL and the thermal noise of the photo receiver.

Bit-Rate

Bitrate and signal quality performance of SDoF for different combinations of symbol rates and modulation formats have also been investigated. Combinations of three different modulation schemes (16, 64 and 256 QAM) and three different symbol rates (250, 500 and 1000 Msym/s) with 12 GHz carrier frequency are used, corresponding to net communication bitrates of 1-8 Gbps.

The results of the measurements are presented in Fig. 2.13 (b). As expected, increasing the modulation order does not effect the EVM performance, however it increases the bit-error rate. For a given SNR, larger modulation orders result in higher BER compared to the smaller ones, due to the condensed constellation points. Moreover, increasing the bandwidth results in EVM degradation, which is due to the constant power budget of the VCSEL. In other words, increasing the bandwidth decreases the in-band power of the sigma-delta modulated signal and with a constant noise floor it results in a higher EVM. Nevertheless, the

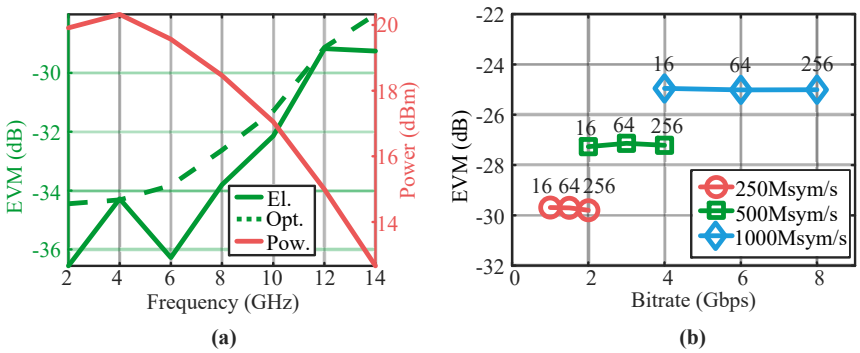

Figure 2.13: (a) EVM of captured symbols at the output of the photoreceiver (Opt.) and output of the pulse-pattern-generator (El.) for different center frequencies. 250 Msym/s symbol rate and 64 QAM modulation is used in order to isolate the effect of carrier frequency. The in-band output power of the pulse-pattern-generator with respect to center frequency is presented in the right axis. (b) Bitrate as function of modulation order and symbol rate. The numbers above the lines represents the modulation orders of 16, 64, 256 QAM.

results show that SDoF can be used to transmit a 8 Gbps modulated signal at 12 GHz carrier frequency with an EVM of -25 dB.

2.5 Discussion

In this chapter, potential and limitations of ultra-high-speed SDoF links with state-of-the-art VCSELs are investigated. First, the effects of VCSEL characteristics on such communication links are investigated by employing three different VCSELs. The signal quality of the SDoF communication link is evaluated under various bias currents and modulation voltages. Then, experiments with different carrier frequencies (2-14 GHz) and bitrates (1-8 Gbps) are performed.

The results indicate that ultra-high-speed SDoF communication links employing state-of-the-art VCSELs can be realized in beyond-10 GHz systems. Employing VCSELs will not only enable low-cost, low-complexity RRHs, but also provide low-energy efficiency and long life span potential. Furthermore, implementation of SDoF also decreases the BER requirements of communication system.

2.6 Potential and Limitations

SDoF provides flexibility in terms of the carrier frequency and symbol-rate. Let us consider a SDoF communication system example with a carrier frequency of 1.5 GHz and operating at 5 Gbps sigma-delta sampling rate. The remote unit consists of: a band-pass switch filter bank [77] with bandwidths matched to the RF-signal at different carrier frequencies and a wideband power amplifier (PA) with a fractional bandwidth of 97% at 2 GHz [78]. The Nyquist sampling theorem tells that, any center frequency up to 2.5 GHz can be employed with 5 Gbps sigma-delta sampling rate. In such a system, the carrier frequency can be easily changed by re-programming the sigma-delta modulator and controlling the switched filter bank. Furthermore, the symbol-rate can also be changed in

a similar way as long as the quantization noise does not become the limitation. The system can therefore be easily reconfigured in a cost efficient way.

SDoF is not limited to binary communication, since the SDM can generate signals with more than one discrete level. However, all the developments of high-speed digital interconnects and constantly increasing clock rates of FPGAs make binary SDoF more appealing. Thus, the work presented in this thesis focuses on two-level, i.e. binary, SDoF communication links.

One of the major advantages of SDoF is that the up-conversion is performed in digital domain at the CU. First of all, this decreases the cost, complexity and the package size of the remote unit by eliminating the traditional analog mixer and local oscillator stages. Furthermore, this facilitates fully synchronous communication links for systems that require phase coherent transmission from physically separated remote units. This will be further discussed in the following chapter.

Chapter 3

Distributed Antenna System based on Sigma-Delta-over-Fiber

With 5G and beyond, both the number of users and the number of devices connected to the network is projected to increase tremendously [79]. Cell densification is one of the methods to address the expected increase of the service demand in the cellular network [80]. Cell-free massive MIMO [81], distributed-MIMO [82], C-RAN [83,84] are some of the major architectures that can be employed for cell densification. A common feature of these methods is that all the complicated signal processing operations are performed at a central location, CU, thus enabling many connected low-complexity remote antennas, remote radio heads. The RRHs have to be low-cost, low-complexity, scalable and flexible in order to execute the required massive upgrade of the network systems. Furthermore, to benefit fully from the joint transmission/reception of the signals RF-phase coherency between multiple, spatially distributed RRHs is required. For such networks, RoF is one of the most pronounced techniques used to form the communication links between the CUs and the RRHs.

SDoF, which was described in detail in the previous chapter, addresses many of the aforementioned requirements, thanks to providing low-cost, low-complexity, RF-phase coherent RRHs [45]. In this chapter, the potential and the limitations of SDoF for emerging and next generation cellular networks are evaluated through the development of a distributed multi-antenna testbed based on SDoF [Paper C]. Then, the experimental results of co-located and distributed MIMO [Paper D] and energy transfer [Paper E] are discussed. The section starts with a brief introduction to distributed MIMO communication together with testbeds previously reported in literature.

3.1 Distributed MIMO

A conventional MIMO base-station that has many closely located (transmitter) antennas can lead to highly correlated channels [85]. In such a scenario, where different channels are highly correlated, the capacity reduces significantly [86],

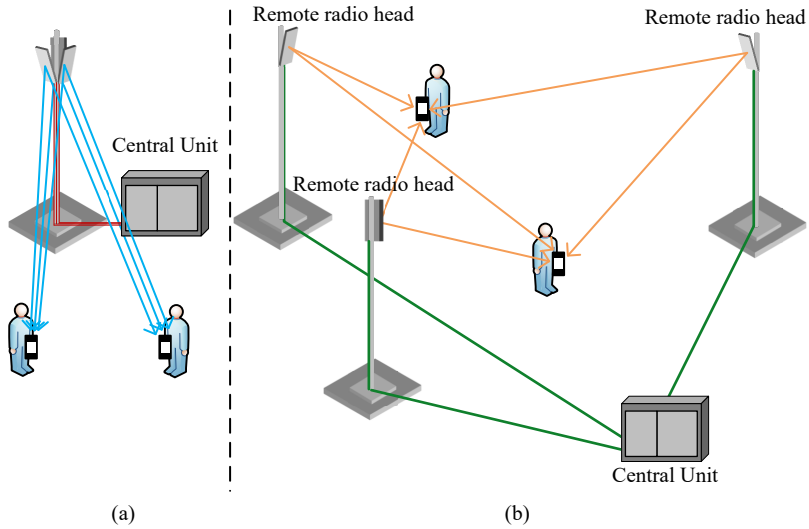

Figure 3.1: Illustration of downlink communication of conventional co-located MIMO (a) and distributed MIMO (b) system.

which yields poor reliability and reduced coverage. An alternative method to decrease the correlation, increase the system capacity, improve the coverage, is to distribute the (transmit) antennas, RRHs [87, 88]. In other words, forming a distributed MIMO (D-MIMO) system [89–95].

Tere are many challenges that need to be addressed when it comes to the practical realization of D-MIMO systems. One of the key challenges is the RF-phase synchronization between physically distributed RRHs. Regardless of the distance between (transmission) antennas, any MIMO system requires accurate phase synchronization between antennas/RRHs to perform MIMO techniques such as spatial multiplexing, beamforming, interference nulling, etc. [96].

Fig. 3.1 (a) shows a simplified block diagram of the downlink of a multi-user MIMO (MU-MIMO) communication system with three base-station antennas serving two users. In a nutshell, MU-MIMO is a MIMO technique where a transmitter with multiple antennas serve multiple users with one or more receiver antennas. In Fig. 3.1 (a), the RF signals are transported from the base-station to the antennas at the base-station tower. Signals for different antennas are upconverted with a shared local-oscillator (LO) and mixer at the base-station, providing a phase synchronous transmission. One of the main challenges of forming a distributed MIMO system is to maintain accurate phase synchronization between spatially distributed RRHs. In Fig. 3.1 (b), an example of a D-MIMO transmitter is shown. If the baseband data provided by the CU is upconverted at each antenna tower with individual LOs and mixers, the individual LOs of each RRH will induce a different phase shift, thus eliminating the phase alignment performed by the CU for any joint transmission. Further, LOs can have frequency errors leading to different carrier frequencies after the upconversion. In conclusion, accurate RF-phase synchronization between RRHs is a fundamental challenge in D-MIMO systems due to the large distance between them, requiring additional measures compared to conventional,

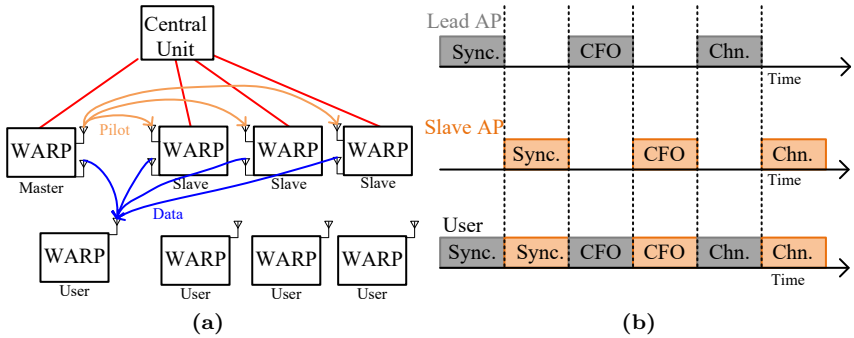

Figure 3.2: (a) The schematic of AirSync D-MIMO system, where one antenna of the slave access point (AP) continuously listens to the pilot transmission from the master AP and the other antenna transmits the information signals to the user. APs are formed by Wireless Open Access Research Platform (WARP). (b) The packet transmission sequence of MEGAMIMO D-MIMO system, symbols in grey are transmitted from the lead AP and symbols in orange are transmitted from the slave AP. Transmission of channel estimation symbols (Chn.) are repeated and interleaved from different APs.

co-located systems, see Fig 3.1.

3.2 Distributed MIMO Testbeds

Different solutions have been proposed to realize distributed MIMO systems with synchronized, coherent RRHs [96–100]. In general, the D-MIMO testbeds provide RF-phase synchronous RRHs either by wireless or by hardware synchronization. Both of these synchronization methods have their own advantages and disadvantages in terms of: additional signal processing, RRH complexity, the possible antenna deployment distance, etc. In the following sections these testbeds are reviewed in terms of their synchronization method and RRH complexity.

3.2.1 AirSync

AirSync [96] was one of the first real-time distributed MIMO communication systems. It employs a wireless synchronization technique to achieve a phase coherent transmission from APs. In AirSync, all the APs are connected to a CU, which is responsible for distribution of the baseband signals, see Fig. 3.2 (a). One of the APs in a cluster, i.e. network cell, is selected as master (reference) AP whereas all the others become slave APs. Every slave AP has two antennas: one dedicated antenna for the reception of the pilot signals transmitted by the master AP and one antenna for the actual information signal transmission. Every slave AP measures the instantaneous phase of the pilot signals transmitted by the master AP and compensates for the drift while transmitting the information signal from the second antenna. The synchronization pilot signals are placed outside the information signal bandwidth, which facilitates a simultaneous transmission and synchronization. The extensive signal processing performed at each AP requires powerful and complicated APs. In AirSync, the APs are

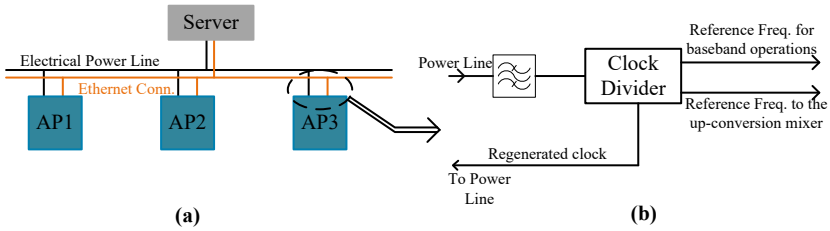

Figure 3.3: (a) Vidyut D-MIMO testbed connection and (b) clock distribution diagram. Three outputs of PLL based clock divider is also presented.

formed by wireless open access research platform (WARP) radio units [101], which consist of FPGAs, RF front-ends, clock boards, etc. Moreover, the pilot transmission from the master AP to the slave APs require them to be within communication range, which can limit the maximum deployment area of the APs. On the other hand, the authors suggest a relay communication method, in which every AP forwards the received pilot signals to the next AP, as a solution for this problem. In summary, AirSync successfully demonstrates synchronized D-MIMO communication through wireless synchronization to the cost of complex signal processing, costly and complicated APs and limited distance for AP deployment.

3.2.2 MegaMIMO and MegaMIMO 2.0

MegaMIMO [97] and MegaMIMO 2.0 [100] also provide phase coherent D-MIMO communication with wireless synchronization. Similar to AirSync, these testbeds also divide the APs in two categories: lead AP and slave APs. The transmission sequence starts with a synchronization header transmitted by the lead AP, see Fig. 3.2 (b). Each slave AP then calculates the phase drift of its LO from the lead APs LO. The predicted phase difference is used later for compensation to achieve coherent data transmission. After synchronization header transmission, lead and slave APs transmit channel measurement blocks one at a time. In this way, the APs do not interfere with each other and interleaving packets provide a close approximation to simultaneous measurement of the channels from all the APs to a client. Finally, the APs use the estimated relative phase offset and the channel state information for a joint data transmission to the clients. The synchronization and channel measurements are repeated according to the coherence time of the channel.

The MegaMIMO system is upgraded with a distributed power control and full-fledged real-time 802.11 PHY in MegaMIMO 2.0. Similar to AirSync, both the MegaMIMO systems require complex and expensive APs in order to perform all the necessary computations required for joint transmission. In MegaMIMO, the APs are formed by USRP2 boards and RFX2400 daughterboards [102]. In MegaMIMO 2.0, the APs are realized by Zedboard [103] connected to an Analog Device FMCOMMS2 transceiver card [104].

3.2.3 Vidyut

A rather different approach than the previous testbeds is used in the Vidyut D-MIMO testbed [99]. In Vidyut, all the APs and the central server are connected to the electrical power lines of the building complex, see Fig. 3.3 (a). These electrical power lines are used to transmit a 10-MHz reference clock from the central server to the APs. At each AP, the reference clock is first bandpass filtered and then fed to the PLL of the clock distribution circuit, see Fig. 3.3 (b). The clock distribution circuit has three outputs: one is used as clock for baseband operations, the second output is fed to the up-conversion mixers and the third output is fed back to the power lines to overcome the attenuation of the power distribution network. At each AP there is also an isolation transformer to protect the circuit from the high voltage of the electrical power lines. For the transmission of baseband data, another link between the central server and the APs is established with an ethernet connection. The APs of the Vidyut are formed by NI-5791 [105] radio front-ends, which are also equipped by a PLL based clock distribution core AD9511. Compared to previously mentioned testbeds, Vidyut requires less complex and cheaper APs. However the main drawback of Vidyut is that the system depends on the established electrical power lines.

3.2.4 Zinwave and PCell

There are also commercial products such as Zinwave [106] and Pcell [107] for realizing D-MIMO communication systems. Generally, these products are closed systems and developed to meet a specific standard, for example PCell is developed for LTE communication standards. Thus, these products are not suitable for research of new D-MIMO communication concepts beyond currently existing standards and use cases.

3.3 Distributing Antennas Through Sigma-Delta-over-Fiber

The testbeds mentioned above successfully demonstrate the capabilities and benefits of distributed MIMO for emerging cellular network systems. However, these are aimed for real-time communication systems and not completely flexible in terms of carrier frequency, symbol rate, modulation order, number of transmission channels, etc. Furthermore, SDoF naturally provides RF-phase coherency, since the up-conversion in digital domain is performed with the same digital clock at the CU. Additionally, the bi-level nature of SDoF communication facilitates the use of low-cost, low-dynamic range optical components produced for high speed datacom applications. Overall, SDoF eliminates any extra efforts for the synchronization and provides low-complex, low-cost RRHs with a capability of joint central coordination of the system.

The testbed [Paper C] presented in the following sections is aimed to demonstrate the potential and limitations of SDoF for distributed antenna systems. Likewise, it is designed to serve as a platform to conduct measurements and for analysis of distributed antenna systems in real environments due to

it is flexibility. To the best of the author's knowledge, [Paper C] is the first demonstration of a SDoF based distributed MIMO testbed.

It is also worth to mention that, SDoF is not only limited to forming testbeds for experimental analysis. Recent publications have shown that it is possible to implement real-time SDoF distributed MIMO. In [43], a real-time, distributed MIMO system based on RF-SDoF is demonstrated. It provides two phase coherent transmission channels and performs real-time LP-SDM at the CU FPGA unit. The system is evaluated through signals centered at 3.5-GHz with 40.96-MHz and 163.84-MHz bandwidths. A mmWave SDoF distributed MIMO system is presented in [46]. As mentioned previously, a SDM IF-signal is transmitted through optical fibers and the upconversion to the 25-GHz center frequency is performed at the RRH. Although upconversion is performed with individual LOs, it offers RF-phase synchronous RRHs by recovering the LO-signal from the received IF-signal. However, compared to direct RF signal transmission through the optical fiber, this method suffers more from phase noise.

3.4 Proposed Testbed

Fig. 3.4, shows the schematic of the proposed testbed [Paper C]. In its current implementation, it provides twelve RF-phase coherent downlink channels and offers great flexibility in terms of signal properties such as carrier frequency, bandwidth, modulation format, etc. Overall, it is a low-cost, low-complexity, flexible, fully synchronized platform for distributed antenna experiments.

The testbed hardware can be divided into two parts: The central unit, where all the signal processing, signal generation and electrical to optical conversion is done, and the RRH at the far end of the optical link, where the optical to electrical conversion, bandpass filtering, amplification and antenna transmission is performed.

3.4.1 Central Unit

The central unit is realized by an FPGA development board (Transceiver Signal Integrity Development Kit, Stratix V GT Edition). The FPGA board has 28 $\times$ 12.5 Gbps and 4 $\times$ 28 Gbps high speed transceivers.

To synchronize all the communication links for a coherent transmission, a 625-MHz external master clock is connected to the FPGA development board. Two PLLs, each serving six channels, are synchronized to the same master clock, which provides twelve RF-phase coherent transmitter channels.

Twelve, upconverted and oversampled RF signals are sigma-delta modulated (2^{nd} order) with MATLAB delta-sigma toolbox [29] and uploaded to twelve random-access-memories (RAM) of the FPGA board. The FPGA board continuously reads the data from the RAMs and transmits them to small form-factor pluggable transceivers (SFP+, Avago AFBR-709SMZ). The optical signals, converted by the SFP+ transceiver modules, are transmitted to another SFP+ module at the RRH through a 30m OM4 multi-mode fiber (MMF). The SFP+ transceivers support a maximum transmission rate of 10 Gbps with a maximum distance of 300 meters. In other words, the current testbed configuration enables approximately 600m coverage.

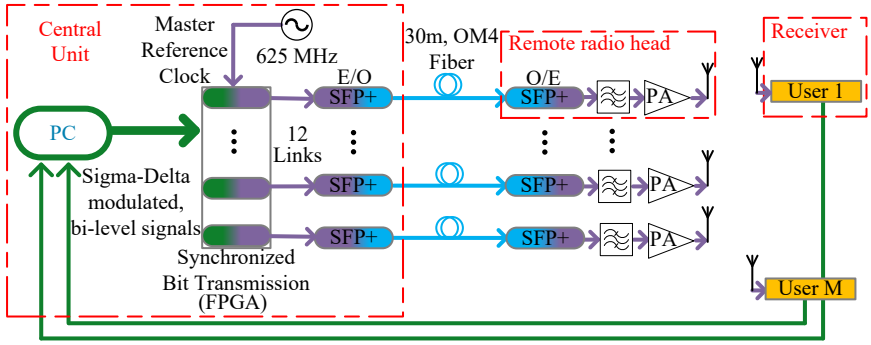

Figure 3.4: The schematic of the presented sigma-delta-over-fiber based D-MIMO testbed. Twelve bandpass sigma-delta modulated bit-streams are created in MATLAB and uploaded to the FPGA. The output of twelve multi-gigabit transmitters of the FPGA are converted to the optical domain with SFP+ modules followed by 30m, OM4, multi-mode fiber (MMF). The received signal at the RRHs is converted to electrical domain with SFP+ modules. Then, the RF-signal is recovered from the bitstream with bandpass filters. Finally, the recovered RF-signal is amplified with PA and transmitted with a patch antenna. The receiver/client is formed with an signal analyser (Agilent N9030A) controlled by the same PC.

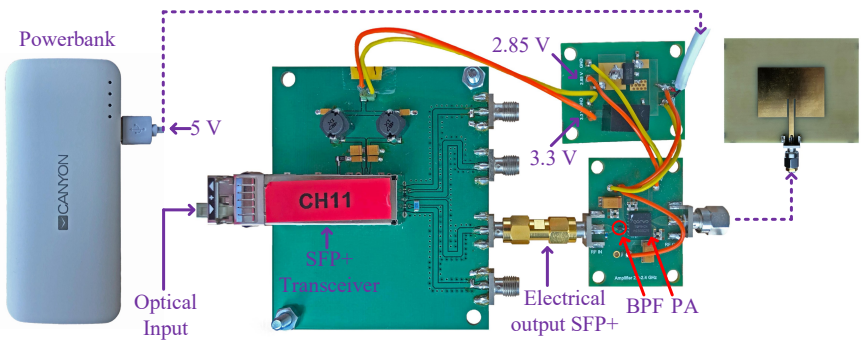

Figure 3.5: Photo of one of the twelve identical RRHs. First, the received optical signal is converted the electrical domain by using an SFP+ transceiver. Thereafter, the signal is bandpass filtered and amplified before the transmission with a patch antenna. A powerbank with 5 V output in combination with two different voltage regulators (2.85 V and 3.3 V) is used as a power source.

3.4.2 Remote Radio Head

At the RRH, first the received optical signal is converted to electrical domain by an SFP+ transceiver, see Fig. 3.5. Thereafter, the original RF-signal is recovered by a bulk-acoustic wave (BAW) commercial bandpass filter. After the bandpass filter, the signal is amplified with a commercial power amplifier (PA, Qorvo TQP9424), which provides 36 dB gain at the band of interest. Finally, the signal is transmitted by a microstrip patch antenna.

To provide flexible deployment of the RRHs, they are equipped with a DC-power source (USB Powerbank, 5 V, 13000 mAh) and mounted into plastic boxes. The required supply voltage levels at the RRHs are supplied from two different voltage regulators (2.85 V and 3.3 V). In this way, more than 10 hours of operating time is achieved without any need of external power supply.

3.4.3 Flexibility

Integrating the SDoF technique with distributed MIMO systems not only provides RF-phase synchronous RRHs, but also enables flexibility throughout the system in terms of the hardware, signal processing algorithms and signal parameters. Various signal processing algorithms, including channel estimation, precoding, etc., can be implemented, since the testbed offers offline processing. The digital up-conversion at the CU enables the carrier frequency to be changed only by replacing the bandpass filter and changing sigma-delta modulation parameters. The implemented FPGA and SFP+ are able to support up to 10 Gbps bitrate, enabling carrier frequencies up to 5 GHz. The current FPGA platform supports up to 28 synchronized channels. Moreover, the implemented FPGA supports four channels with 28 Gbps maximum bit-rate. Simply replacing the SFP+ transceivers with QSFP+ modules, which support up to 40 Gbps optical communication, these four channels of the FPGA can be used. This upgrade enables carrier frequencies up to 14 GHz at four coherent transmission channels.

The number of channels, maximum carrier frequency and symbol rate can be easily increased as more advanced FPGAs are available. For example, one of the newer FPGAs from Intel (Stratix 10 TX), supports up to 120 GXE transceivers, each with a maximum bit-rate of 30 Gbps.

The flexibility of the current testbed in terms of the carrier frequency and symbol-rate is demonstrated in the following section.

3.4.4 Single Link Evaluation

The in-band quantization noise power of a SDM is independent of the chosen carrier frequency in the first Nyquist zone [29]. Hence, different carrier frequencies can be realized merely by changing the sigma-delta modulator parameters at the central unit and the bandpass filter at the RRH. As mentioned previously, switched filter banks can be a solution to dynamically control the band of operation.

The carrier frequency flexibility of the testbed is demonstrated through measurements. Signals centered at different center frequencies are transmitted and the normalized mean squared error (NMSE) of the transmitted symbols are calculated. During the measurements a default symbol-rate of 10 Msym/s and

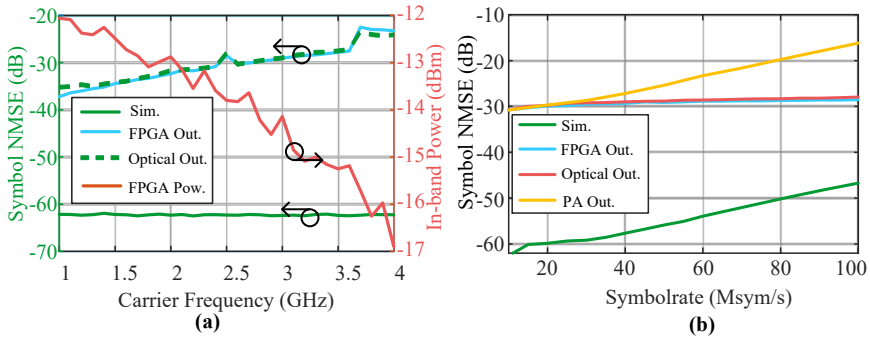

Figure 3.6: (a) Error-vector-magnitude of transmitted symbols measured at the output of the FPGA (Elec.) and at the electrical output of the SFP+ located at the RRH (Opt.). The in-band output power of the FPGA with respect to frequency is presented on the right axis. (b) Measured error-vector-magnitude at the output of the SFP+ (Meas.) compared with simulated (Sim.) for different symbol-rates.

64-QAM modulation format is considered. The receiver instrument is directly connected to the output of the FPGA. In order to discover any possible effects of the optical link, the same measurements are performed at the electrical output of the SFP+ at the RRH, see Fig. 3.4.

The NMSE of the transmitted symbols and the in-band output power of the FPGA versus the carrier frequency is presented in Fig. 3.6 (a). Despite the theory [29], the NMSE of the transmitted symbols increases versus carrier frequency. This can be explained by the decreasing output power of the FPGA at higher carrier frequencies. In other words, the lower output power with a constant FPGA noise power leads to SNR degradation, which results in higher NMSE. The NMSE measured at the output of the SFP+ shows that the signal quality, is not degraded by the optical link. This indicates that the optical interface has a lower noise level than the FPGA, thus the NMSE is preserved throughout the optical link. In conclusion, the FPGA frequency response limits the performance. Nevertheless, even for the highest tested carrier frequency, NMSE of the transmitted symbols is $\sim$ -25 dB.

Another flexibility of the testbed is demonstrated by transmitting signals with different symbol rates, centered at 2.365 GHz. The transmitted signals are acquired at three different points in the communication chain: the output of the FPGA at the CU, the output of the SFP+ and the power amplifier at the RRH, see Fig. 3.4. Fig. 3.6 (b) shows the measured and simulated NMSE for different symbol rates. The NMSE of the simulated symbols increase for higher symbol rates due to the increased in-band quantization noise [29] and decreased signal spectral density. On the other hand, large oversampling ratio, i.e. very low in-band quantization noise due to large oversampling, and the noise power level of the FPGA makes this invisible in the measurements. This results in a constant signal quality with respect to symbol-rate.

The fact that we observe similar results before and after the optical link shows that the optical link does not degrade the signal quality. However, a significant signal quality deterioration is observed at the output of the power amplifier when the symbol-rate is increased. The optical output of the SFP+ at the RRH (red curve at Fig. 3.6 (b)) is connected to a BPF and a power

amplifier, see Fig. 3.4, which indicates the degradation is caused by either of these components. Despite extensive investigations, the exact cause of this problem could not be determined. In addition, it was not necessary to change these components, as there was no reduction in signal quality for the chosen bandwidth (10-MSym/s), which is required in the measurements mentioned in the rest of the thesis. The signal quality degradation is related to the components employed rather than the proposed architecture. If it is necessary to employ higher bandwidths, this effect can be easily solved with replacing the aforementioned components.

3.5 Communication Experiments

This section presents the results of communication experiments performed with the complete proposed testbed, in which the D-MIMO is compared wiht the co-located MIMO (C-MIMO) antenna deployment in a real environment [Paper D].

3.5.1 Measurement Method

The comparison experiments are performed in a laboratory providing a rich scattering environment with tables, measurement racks, cabinets, etc, see Fig. 3.7. The same signal analyser used for verification measurements is formed the receiver with a mono-pole WiFi antenna. Each RRH is mounted to the walls, as shown in Fig. 3.7, approximately two meters above the floor. All measurements are performed with a 16-QAM, 5-Msym/s RF-signal centered at 2.365 GHz and modulated with 2^{nd} order bandpass sigma-delta modulator.

Measurements are conducted in 31 different locations. At each location first single user, then multi-user MIMO communication experiments are performed. Each measurement starts with a channel estimation phase to calculate the channel matrix. After the estimation of the channel matrix, first single user measurement with beamforming precoding, then two and three user measurements, i.e. MU-MIMO, with zero-forcing beamforming (ZFBF) precoding are performed. During two- and three-user measurements, one of the clients is always formed by the receiver at the current location and the other clients are randomly picked from the previously measured locations. At every location, up to 8 different two-user and three-user measurements are performed, resulting in 31, 212, 212 unique 1-, 2-, 3-user measurements, respectively, for C- and D-MIMO. The details of the measurement methodology are presented in [Paper D].

At the end of these measurements, the co-located and distributed MIMO are compared in terms of the received power, received symbol EVM and inter-user interference.

3.5.2 Multiple-input-single-output (MISO)

Fig. 3.7 shows the measurement lab and the 31 measurement locations used in the experiments. The received power of both C- and D-MISO is also presented. The distribution of the received power across the room is presented in Fig. 3.8. Both figures show that, distributing the RRHs increases the received power,

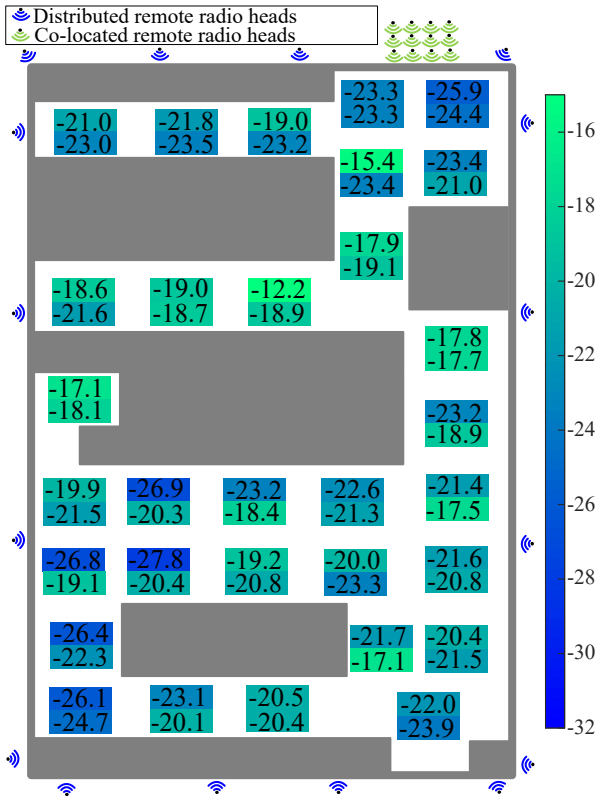

Figure 3.7: Illustration showing the measurement locations in the laboratory and the received powers for single user experiments. At each box, bottom value and top value represents distributed and co-located RRHs, respectively.

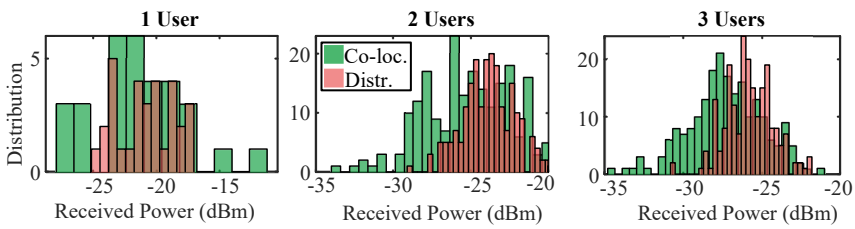

Figure 3.8: The distributions of the received power throughout the measurement laboratory for different number of users.

thus resulting in improved coverage in the room. It is worth mentioning that, in certain receiver locations co-located MISO delivers higher power, especially when the receiver is in the line-of-sight of the closely located RRHs. However, in some locations the received power decreases significantly compared to D-MISO. In summary, D-MISO outperforms C-MISO in terms of higher average received power.

In Table. 3.1 the average EVM of the received symbols is presented for both C- and D-MISO. Despite the different average received power levels, the EVM values of the signals are similar. This is mainly due to the high sensitivity of the receiver instrument and the relatively small size of the measurement laboratory.

Table 3.1: Average error-vector-magnitude (EVM) and signal-to-interference ratio (SIR) of different number of users for distributed and co-located MIMO.

	EVM (dB)		**SIR (dB)**	
	Distr.	Co-loc.	Distr.	Co-loc.
1-User	-28.4	-27.4	-	-
2-Users	-22.0	-20.4	23.2	22.8
3-Users	-18.7	-17.4	19.6	19.4

3.5.3 Multi-User Multiple-input-multiple-output (MU-MIMO)

Fig. 3.8 presents the received power distributions of all 212 measurements conducted with 2- and 3-users for C- and D-MIMO. Similar to the MISO case, distributed MU-MIMO delivers more uniform power levels compared to co-located MU-MIMO. The average EVM and signal-to-interference ratio (SIR) is presented in Table 3.1. The results show that distributing the RRHs and forming a D-MIMO system can improve the EVM and SIR compared to C-MIMO. The main reason of EVM degradation when the number of users is increased, is the residual interference. Theoretically, ZFBF eliminates all the inter-user interference with a perfect CSI [108]. However, the imperfect channel estimation results in interference residuals, which explains the EVM degradation.

In [Paper D] another MU-MIMO precoding technique, maximal-ratio-combining (MRC) [109] is implemented. MRC is a precoding technique that maximizes the receiver power at each user without considering the inter-user interference. In general, ZFBF pre-coding is implemented if the communication system is interference limited while MRC is used for signal-to-noise ratio (SNR) limited scenarios. The experiments in [Paper D], show that the communication system is highly interference limited. This is mainly due to the relatively small size of the measurement laboratory. Therefore, further experiments are not performed with MRC precoding.

Overall, the experimental results show that the distributed-MIMO provides better signal quality and higher received power compared to co-located MIMO. Furthermore, the experiments demonstrate the potential of the sigma-delta-over-fiber for distributed MIMO communication.

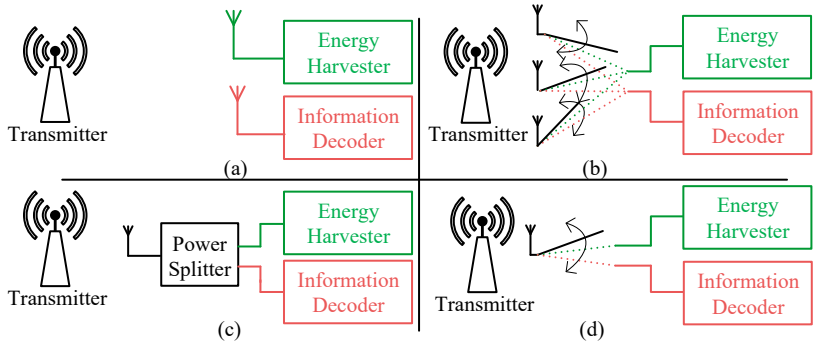

Figure 3.9: Block diagram of four different simultaneous wireless information and power transfer (SWIPT) receiver architectures.

3.6 Wireless Power Transfer

As mentioned before, with 5G and beyond the number of devices connected to the network will increase drastically. However, it is not only the number of devices that is increasing, but also many different types of devices such as, wearables, cars, sensors, etc. will be connected to the network system. Many of these remote nodes will be operated through batteries. Charging these batteries might not be possible due to high mobility and/or environmental access difficulties. Technologies to facilitate recharging these batteries in a green way and reduce costs have attracted a lot of attention in recent years. Energy harvesting is a method, which uses environmental energy sources, namely sound, heat, RF, light to charge such batteries [110]. Wireless power transfer (WPT), which utilizes ambient or dedicated radio signals to generate DC-power, is a very promising technique for wireless communication networks due to its stable and accessible nature [111].

The simultaneous wireless information and power transfer (SWIPT) technology provides a solution by sending both the information RF signal and the signal that is used to charge the batteries simultaneously [112]. SWIPT is highly suitable for wireless network systems since it preserves the signal quality while enabling DC-power generation.

It is no longer possible to think of 5G and the next generation mobile network technologies independently of MIMO. Therefore, it is necessary for a SWIPT system to be suitable to work with MIMO architectures. In general, energy transfer efficiency is heavily dependent on the user's location. As the user is away from the transmitter antennas, the DC power generated decreases due to the received energy level [113]. However, energy transfer efficiency can be increased if the antennas are physically distributed and a distributed MIMO system is formed [114,115]. In the previous chapter, it is shown through experiments, that D-MIMO increases the received power in the communication environment. In short, a SWIPT system benefits from distributed transmitter antennas, and this has been experimentally demonstrated with the SDoF testbed.

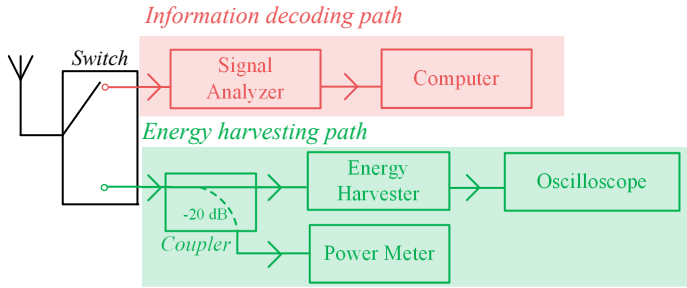

Figure 3.10: The block diagram of the receiver architecture for the simultaneous wireless information and power transfer (SWIPT) experiments. The red path shows the communication signal receiver whereas the green path presents the DC-power generation through energy transfer.

3.6.1 Simultaneous Wireless Information and Power Transfer Architecture

In the SWIPT architecture, the receiver must generate DC-power while maintaining the required communication signal quality. Hence, the received signal must be divided in to two separate parts for energy transfer and information decoding. There are four main structures in the literature to perform such separation successfully, illustrated in Fig. 3.9. The most straightforward method is to have separate receivers with their own antennas for the energy transfer and information decoding, see Fig. 3.9 (a). The separate antennas might degrade the beamforming performance of the transmitter, since the channel will be estimated with the information receiver antenna. On the other hand, it provides independent and uninterrupted energy transfer. A more complex method is presented in Fig. 3.9 (b), which utilizes two different subsets of antennas at a given time for energy transfer and information decoding through an antenna switching circuitry. In this way, a certain number of antennas can be dedicated to either information decoding or energy transfer, depending on the communication or WPT requirements. The third method is presented in Fig. 3.9 (c). It utilizes a power splitter, which connects the receiver antenna/antennas to the RF-to-DC converter and the information decoder circuitry. In the power splitting method, the power splitting ratio can be adjusted according to the information decoding and energy transfer requirements [111]. In [116] it is shown that the power splitting method provides the best trade-off between information decoding and energy transfer. The final method is time splitting and shown in Fig. 3.9 (d). The receiver antenna/antennas are connected to a switch, which periodically changes the connection either to the energy transfer or information decoding circuitry. Thus, at a given time one of the operations is performed. It is necessary for this method to have an accurate scheduling.

The time switching method is employed for the SWIPT experiments performed with the SDoF testbed. The following section will first present the measurement setup and then the performance will be evaluated using the experiment results.

3.6.2 Experimental Design

The block diagram of the measurement setup is presented in Fig. 3.10. A commercial RF-to-DC converter (PowerCast P21XXCSR-EVB [117]) is utilized to generate DC-power, whereas an Agilent signal analyzer (PXA N9030A) formed the information decoding receiver. The receiver antenna is connected to either of the receivers, i.e. information decoder or RF-to-DC converter, through a manually controlled analog switch (Minicircuits ZMSW-1211) depending on the state of operation. Further, a power meter (Agilent E4419B) is employed to measure the received power level during the energy transfer state and an oscilloscope (Agilent MSO6034A) is utilized to calculate the generated DC-power.

It is worth to mention that, a driver amplifier between the RF-to-DC converter and the receiver antenna is employed during the experiments. The main reason is that, the RF-to-DC converter requires around 10 dBm receiver power level in order generate DC-energy efficiently. The presented experiments aim to demonstrate the capabilities of SDoF D-MIMO communication with SWIPT technologies. In a real communication scenario a different RF-to-DC converter could be implemented with lower receive power requirements [118].

The measurements are performed in the same laboratory presented in Section 3.5.1 with the same antenna deployment, see Fig. 3.7. energy transfer and communication experiments are performed at 25 different locations. A SWIPT experiment at a location consists of three phases:

1. Channel Estimation: This is the beginning phase of an experiment. The communication channel between the 12 physically distributed antennas and the receiver antenna are estimated by using time-orthogonal pilots. At this phase, the receiver antenna is connected to the RF-communication receiver.

2. Precoded Information Transmission: The channel state information is used to beamform the communication signal from twelve antennas to the receiver antenna. The antenna is still connected to the RF-communication receiver and the acquired signals are proccessed to calculate the received signal quality.

3. Energy transfer: Before this phase begins, the antenna is connected to the RF-to-DC converter. An unmodulated continuous wave (CW) signal is beamformed to the receiver antenna using the same CSI estimated at phase 1 to maximize the received power. The output of the harvester is acquired with the aforementioned oscilloscope and the generated DC-power is calculated.

3.6.3 Energy Transfer Results

The communication measurement results are very similar to the results presented in Section. 3.5.2, and therefore not discussed here. The distribution of the generated DC-power through energy transfer with respect to measurement locations is presented in Fig. 3.11. On average 5.88 mW DC-energy is generated throughout the laboratory in the experiments. As mentioned previously, a driver amplifier was employed in the measurements to amplify the received

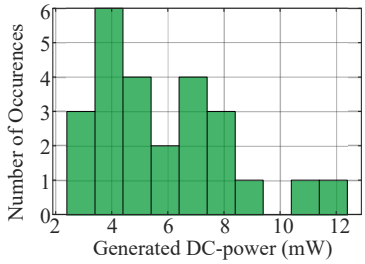

Figure 3.11: The distribution of the generated DC-power through energy transfer throughout the measurement laboratory.

signal used for energy transfer. Thus, the generated DC-energy is not only from the received RF-signal.

Together with the results presented in the previous section, these experiments show that a SDoF based distributed antenna system not only provides good signal quality, but can also be implemented for wireless energy transfer. It is a promising technique to charge the low-power, remote nodes especially since, it provides uniform received power levels. Hence, the charging efficiency becomes less dependent on the location of the user compared to a co-located system.

In some applications, the duration of energy transfer can be much longer than communication phase, depending on the communication requirements. This allows longer times to recharge the battery. In case of multi-users, the system can transmit communication signals to some of the users whilst the others receive energy transfer signals in order to maximize the recharging duration. This can be performed by using multi-user MIMO techniques such as zeroforcing beamforming (ZFBF), maximal ratio combining (MRC), etc.

3.7 Discussion

Sigma-delta-over-fiber is a powerful technique to realize distributed antenna systems since it naturally provides RF-phase coherency between transmitter antennas. In this chapter, the performance of such an architecture, together with the potential and limitations of distributed antenna systems are evaluated through the testbed presented in [Paper C]. The testbed utilizes an all-digital downlink transmission between the CU and the RRHs and provide excellent RF phase coherency between the widely separated antennas. The all-digital nature of the testbed makes it very flexible and future-proof, since it can be upgraded easily when new digital communication technologies such as FPGA, digital optical transceivers, etc, are available. Although, the testbed is designed for experimental evaluation of distributed antenna systems, it also demonstrates the capabilities of SDoF when it comes to forming such systems. The already existing implementations of SDM in FPGAs show that SDoF based distributed antenna systems are also applicable for real-time communication systems.

The benefits of distributing the antennas of a MIMO system in terms of communication coverage and quality-of-service is experimentally demonstrated through the testbed. Simultaneous wireless information and power transfer is

also evaluated with the distributed antennas. Overall, all of these experiments show that the proposed testbed is a very powerful tool for investigating different algorithms, signal properties, antenna deployments in real environments with a large variety of applications such as localization and radars.

Chapter 4

All-Digital Uplink Solution for Distributed Antenna Systems

In Chapter 2, a single ultra-high-speed communication link is realized by state-of-the-art VCSELs to investigate the potential and limitations of sigma-delta-over-fiber communication with ultra-wideband signals. Subsequently, in Chapter 3, an RF-phase coherent testbed is implemented and employed in various distributed antenna system analyses. Overall, it is shown that SDoF offers high signal quality whilst providing low-complexity, low-cost, RF-phase coherent remote radio heads, thus making it highly suitable for emerging and future wireless communication networks. In all of the above mentioned investigations, SDoF is used to form the downlink, from CU to RRH, of the communication systems. An uplink, from RRH to CU, is as important as the downlink in real applications. However, realizing an uplink for a SDoF communication link is not straightforward without compromising its benefits.

In this chapter a novel solution to form an all-digital uplink is presented from [Paper F]. The proposed architecture is extensively investigated through experiments and it is applicable for any radio-over-fiber system utilizing digital signals.

4.1 Radio-over-Fiber Uplinks

In a real network application a radio-over-fiber downlink requires a complementary uplink. For analog-radio-over-fiber architecture the uplink can be realized simply by replicating the downlink but from the RRH to the CU [17], see Fig. 4.1. A local oscillator and mixer stage might be necessary at the RRH, depending on the frequency of operation [119]. The transmission of the RF-signal through the optical link provides low-complexity RRHs with centralized control since all the up/down-conversions are performed at the CU. However, it requires high-bandwidth optical links, which increases the cost significantly. Another drawback of such an architecture is the fiber chromatic dispersion and nonlinear effects of the optical components [19, 20, 120]. Although, there are

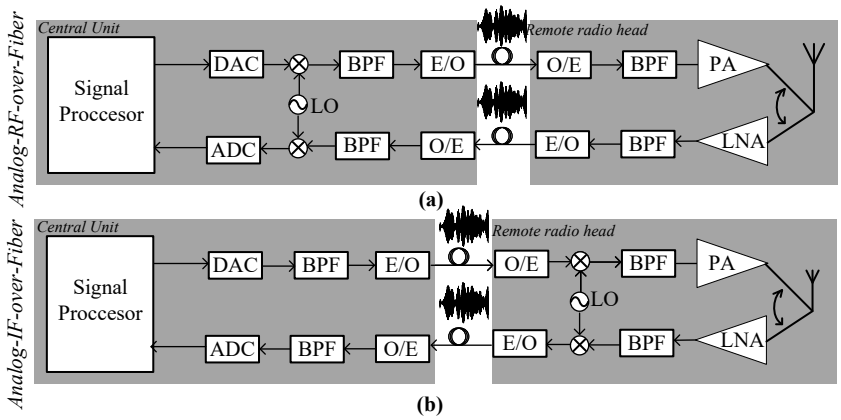

Figure 4.1: The block diagrams of analog-radio-over-fiber architectures. The case where the up-conversion is performed through local oscillators and mixers (a) at the central unit, (b) at the RRH.

methods to linearize an ARoF communication link, it increases the cost and complexity of the system [16, 121–123]. For mm-wave systems an IF signal can be transmitted between the CU and RRHs, as illustrated in Fig. 4.1 (b), in order to mitigate the linearity problem and to decrease the bandwidth requirements of the optical components such as laser and photo-receiver [5,124]. The key issue of such a solution is the up/down-conversion to/from the carrier frequency performed at the RRH. Such an architecture, increases the complexity of the RRHs and requires significant measures to maintain synchronization and coherence between multiple RRHs [17].

As mentioned in Chapter 1, digital-radio-over-fiber is a method utilizing digital signal transmission. In the most straight forward implementation, the frequency conversion to/from the carrier frequency is performed at the CU [21]. A DAC and deserializer is employed to convert the seriliazed and digitized RF-signal to an analog waveform during the downlink phase, see Fig. 4.2 (a). The direct conversion of the received RF-signal to a digital waveform requires a high-bandwidth and power hungry ADC in the uplink phase [125]. Bandpass sampling techniques can be used in order to relax the sampling requirements of the ADC [22, 23]. Another implementation method is to transmit digital baseband signals through the optical link in both down- and up-link phases. This is already a standardized method for cellular networks, e.g. open base station architecture initiative (OBSAI) [26] and common public radio interface (CPRI) [3], see Fig. 4.2 (b). However, as stated many times, this requires LO and mixer stages at the RRH which inherently makes it difficult to have synchronized fully coherent RRHs, which is critical in emerging network systems.

As mentioned throughout the thesis, there are many diversed studies on SDoF downlink architectures. However, none of them offers a solution for the uplink. One of the earliest SDoF studies, proposes implementation of conventional ARoF for the uplink [27], however this is not desirable as mentioned previously.

In [126], an uplink solution based on pulse-width modulation (PWM) is

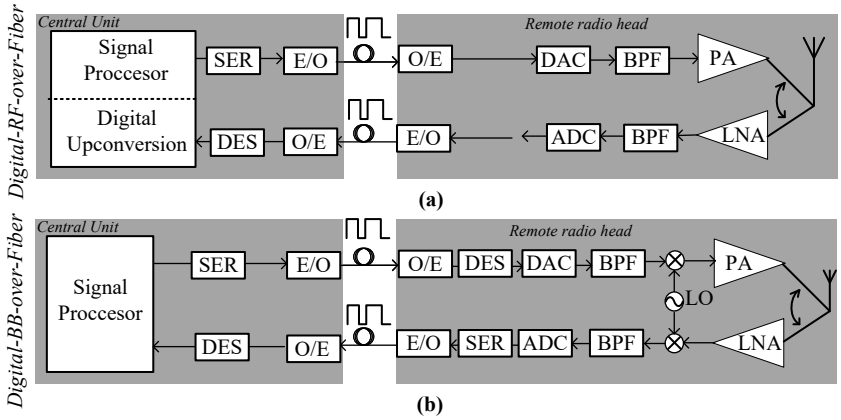

Figure 4.2: The block diagrams of digital-radio-over-fiber architectures. (a) The up-conversion is performed in digital domain at the central unit, (b) a baseband signal is transmitted through the optical link and up-converted at the RRH through local oscillators and mixers.

proposed for binary RoF communication links. In a nutshell, it utilizes a comparator together with a signal generator at the RRH in order to quantize the received RF signal into a binary bitstream. However, generating the reference signal at the RRH increases the complexity and cost of the RRHs. Furthermore, such an implementation is not flexible due to the fixed reference signal and it is also not scalable to systems with many RRHs.

In summary, the conventional uplink methods either require costly optical components, ADCs, or additional complicated procedures to synchronize the RRHs. Hence, employing such structures will compromise many of the benefits of SDoF. In [Paper F], all of these are addressed and a low-complexity, all-digital uplink architecture suitable for emerging wireless networks is proposed.

4.2 Proposed Architecture

An RF sigma-delta-over-fiber downlink provides RF-phase coherent and low-complexity RRHs, since all the frequency shifting operations, e.g. up- down-conversion, as well as signal processing, and time-domain sampling are done at the CU. Naturally, a complementing uplink method has to perform all the above-mentioned processes at the CU. In other words, an architecture which directly transforms the received RF-signal at the RRH to a binary signal without any extra signal processing or frequency shifting operations is desired. The proposed link structure addresses this by comparing the received RF-signal with a reference signal through an analog comparator at the RRH.

Similar architectures are previously used in different applications. In [127], the receiver is formed by an high-speed comparator generating the pulse-width modulated (PWM) RF signal, which is later processed in an FPGA. In [128] and [129], the direct RF-sampling through high-speed comparators is employed to realize digital receivers of software-defined radios (SDR). In all of these studies, it is shown that direct RF-sampling method provides flexibility and agility, due to its all-digital nature.

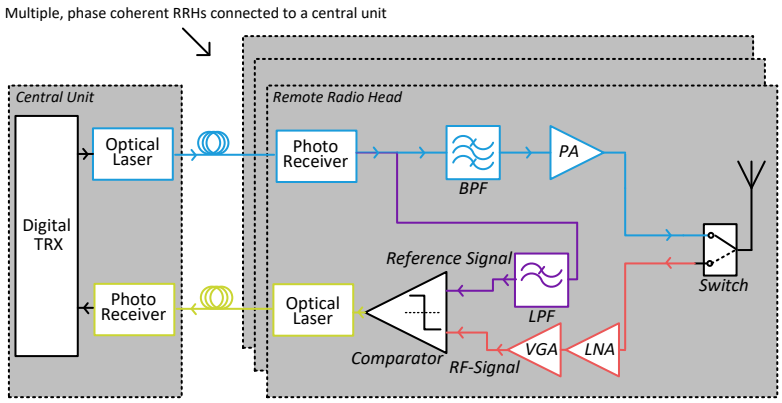

Figure 4.3: The block diagram of the proposed binary radio-over-fiber communication link including the uplink architecture. The blue colored path represents the downlink, the purple color is the part of the downlink utilized as the reference signal transmission during the uplink. The orange path is for the RF signal, and the yellow path is the binary optical uplink.

A general block diagram of the proposed communication system including the uplink is presented in Fig. 4.3. The downlink is formed by a bandpass sigma-delta-over-fiber link. The digitally upconverted signals are first SDM, and then converted into optical domain through a laser. At the RRH, first, the signal is converted back to the electrical domain. Then, the binary signal is bandpass filtered to recover the RF-signal, amplified and transmitted from an antenna. A detailed investigation of such an implementation is presented in Chapter 2 and 3. Hence, the remaining parts of this chapter solely focus on the uplink.

4.2.1 Uplink

In the uplink phase, an analog comparator is used for directly quantizing the received RF signal into a binary signal stream, see Fig. 4.3. The comparison is made against a tailored reference signal in order to maximize the signal quality. The basic principle behind the method is to generate a PWM signal whose duty cycle is determined by the instantaneous voltage difference between the two input signals. The binary output of the comparator is transmitted through a dedicated optical link to the CU, where it is sampled by a digital receiver and processed to retrieve the information data.

The reference signal plays a very important role in the procedure of PWM signal generation, i.e. the quantization of the received RF-signal. Three main properties of the reference signal have a significant effect on the overall signal quality of the uplink: the type of the waveform, the frequency, and the amplitude.

- Waveform shape: An equal quantization of the received signal through comparison requires a reference signal with uniform voltage distribution [130]. Hence, triangular or sawtooth signals are typically preferred.

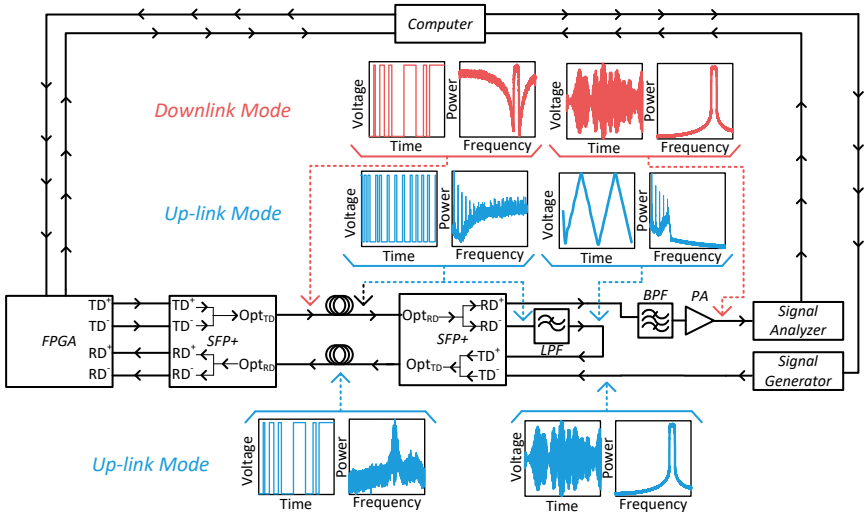

Figure 4.4: The block diagram of the laboratory prototype of the proposed all-digital, time-domain duplex, radio-over-fiber architecture. The time domain signals and corresponding frequency spectra are also shown at different points of the communication links.

- Frequency: The waveform shape and its frequency determines the harmonic contents of the pulse train at the comparator output. The frequency has to be chosen carefully, since the harmonic contents of higher Nyquist zones will be folded to the first Nyquist zone after the sampling at the CU [129]. An inappropriate choice of the reference signal frequency can result in folding of undesired signals to the band-of-interest, thus a substantial degradation of the signal quality.

- Amplitude: The duty cycle of the PWM output of the analog comparator is determined by the instantaneous voltage difference between the RF and reference signal. A very large or very small power level of the reference signal relative to the RF will result in poor quantization of the signal hence degrade the uplink signal quality.

The method of utilizing an analog comparator to directly quantize an RF-signal into a binary PWM sequence is analyzed in [129], where guidelines for choosing the reference frequency as well as its effect on signal quality are presented.

One of the main difficulties of such PWM uplink architectures, is the transfer of the reference signal to the RRH. The proposed solution overcomes this problem by utilizing the downlink for the reference signal transmission. During the uplink phase, the reference signal is generated at the CU and transferred to the RRH through the idle downlink, see. Fig. 4.3. Naturally, such an implementation is suitable for time-divison duplex (TDD) systems. A low-pass SDM is used to encode the reference signal into a binary stream, since the downlink provides a binary communication link. The reference signal is then recovered at the RRH through an analog low-pass filter. Overall, the proposed method establishes extremely simplistic RRHs while providing a digital communication link, suitable for low cost fiber optics, between the CU and the RRH. A digitally controlled switch connects the antenna to the

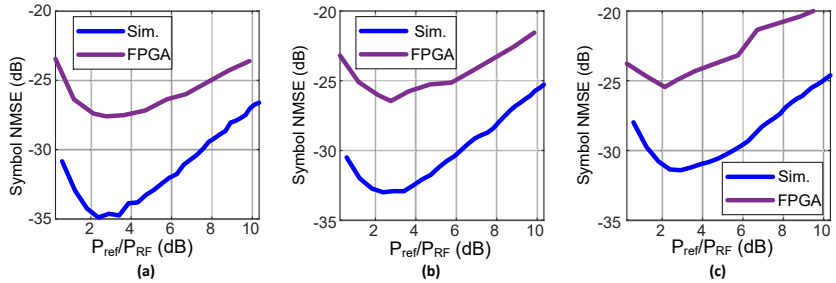

Figure 4.5: The calculated symbol NMSE of the proposed uplink with respect to different symbol-rates, (a) 10-Msym/s, (b) 15-Msym/s, and (c) 20-Msym/s. Simulated (Sim.) and the measured values with the FPGA as the receiver are shown.

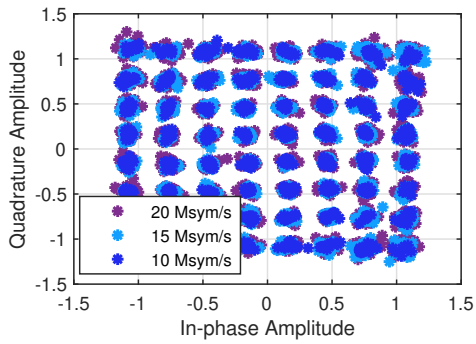

Figure 4.6: The received constellation diagrams for three different symbol-rates with the optimal amplitude ratios between the RF and the reference signal.

downlink or the uplink depending on the phase of the operation. An extra communication link can be used to transfer the reference signal from the CU to the RRH, which eliminates the TDD restriction.

4.3 Implementation Example

A laboratory prototype of the proposed link architecture is implemented in order to evaluate its performance, see Fig. 4.4. The CU is formed by the FPGA, like was presented in Chapter 3. The optical interface between the CU and the RRH consists of a 30m, multi-mode fiber and an SFP+ optical transceivers (Avago AFBR-709 SMZ).

The SFP+ is highly suitable for such an architecture, since it provides differential inputs and outputs, see Fig. 4.4. At the RRH, one of the differential outputs of the SFP+ is connected to a BPF and PA, and used for the downlink communication. The other output is employed together with a LPF during the uplink phase as the reference signal path. The electrical inputs of the SFP+ is connected to the output of the LPF and the RF-signal and used as the comparator to generate the PWM signal.

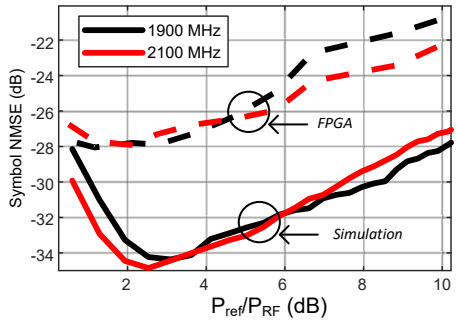

Figure 4.7: The calculated symbol NMSE of the proposed uplink with two different carrier frequencies.

4.3.1 Experimental Results

During the uplink experiments, a signal generator formed the user equipment and the uplink performance is evaluated with various signal parameters. A 20-MHz, SDM triangular signal is transmitted from the CU to the RRH, filtered with LPF and used as the reference signal. Three different symbol-rates (10, 15 20 MSym/s) at 2.365 GHz carrier frequency and two different carrier frequencies (1.9 and 2.1 GHz) with 10 MSym/s symbol-rate are used as the communication signals during the experiments. In all of the above measurements, 64-QAM modulation format and a RRC filter with 0.2 roll-off factor is employed.

As mentioned previously, the power of the reference signal has a significant impact on the signal quality. The symbol NMSE results of the simulation and the measurements with different symbol-rates with respect to power ratio between the reference signal and the RF-signal are presented in Fig. 4.5. There is an optimum power ratio that results in the highest signal quality. The constellation diagram of the received signals at the optimum power ratios are presented in Fig. 4.6. As can be appreciated from Fig. 4.5, this ratio is not effected by the symbol-rate. Furthermore, it is clear that increasing symbol-rate degrades the signal quality for the given parameters. This is mainly due to the constant power budget of the transmitter. Higher symbol-rates decrease the in-band output power, which degrades the total SNR of the signal. Nonetheless, the measurement results show that a good signal quality of -25 dB NMSE can be achieved with highest tested symbol-rate of 20 MSym/s.

The effect of the carrier frequency on the signal quality for the proposed architecture is presented in Fig. 4.7. Similar to the symbol-rate, the carrier frequency does not affect the optimum power ratio. Further, for a given power ratio the two tested carrier frequencies result in very similar signal qualities.

In [Paper F], the proposed architecture is more extensively investigated. For example, the same uplink experiments are performed with a real-time oscilloscope in order to identify any possible degradation caused by the digital FPGA receiver. In these experiments, a better signal quality is achieved and this shows that the proposed architecture is not limited to the presented signal quality levels.

4.4 Discussion

The proposed all-digital, RoF receiver architecture is very flexible thanks to its centralized structure. First of all, many different reference signals and frequencies can be used just by replacing the low-pass filter utilzed to recover the waveform at the RRH.

As shown in the results, the signal quality of the uplink architecture is sensitive to the ratio between the RF-signal and the reference signal. As in conventional receivers, this requires a variable gain amplifier after the LNA at the receiver chain to maximize the dynamic range of the uplink. To some degree, the proposed architecture is able to relax the requirements of the receiver gain control, since the reference signal power level can be adjusted from the CU to a certain extent. The optimum power ratios resulting in the highest signal quality can be stored in a look-up table and used to adjust the coarse gain settings of the gain of the VGA and the reference power level from the CU.

The proposed architecture can provide RF-phase coherency between many, physically separated RRHs, since the reference signals used in the quantization are generated from the same clock source at the CU.

Overall, the experiments show that the proposed architecture is able to present good signal quality while providing extremely simple RRHs. Furthermore, it is shown that the main limitation of the signal quality is the specific implementation rather than the method. In other words, the architecture has a greater potential than what is presented. Moreover, the uplink method is not only limited to systems with SDoF downlinks, it can be used in any system with a digital optical interface between the CU and the RRH.

In conclusion, in this chapter an all-digital receiver/uplink solution suitable for systems with SDoF downlinks is demonstrated. As mentioned previously, emerging and future wireless networks will be composed of many RRHs controlled from fewer CUs. The proposed architecture is suitable for such architectures thanks to its centralized nature.

Chapter 5

Conclusions

In this thesis, the potential and limitations of sigma-delta-over-fiber communication for emerging and future wireless applications have been investigated. The work presented in this thesis can be divided in three main categories: a solution for transferring beyond 10-GHz wideband signals from central units to remote-radio-heads, a flexible and centralized distributed antenna system without any extra measures for RF-phase synchronization and, finally, a complementary uplink solution from the remote-radio-heads to central units suitable for sigma-delta-over-fiber downlink systems.

First, an ultra-high-speed SDoF link is realized by using state-of-the-art VCSELs. VCSELs are highly beneficial for realizing such links, since they provide low power consumption, high-bandwidth density, low manufacturing and packaging costs. VCSELs are mostly used in optical digital communication systems due to their low-dynamic range. On the other hand, this is not a problem for SDoF thanks to its binary nature. Combining these technologies is a powerful method to overcome the constant demand of increasing the communication bandwidth, and enabling beyond 10-GHz carrier frequencies. In order to employ VCSELs in SDoF links, the effects of their characteristics under wideband signals must be known. In this thesis, this is addressed and three different VCSELs with different oxide aperture sizes are employed with various bandwidths, modulation types and carrier frequencies. The signal quality is evaluated under different bias currents and modulation voltages. The results show that VCSELs can be employed in ultra-high-speed SDoF communication links with beyond 10-GHz signals. The integration will not only enable low-cost, low-complexity RRHs, but also provide low-energy efficiency and long life span potential. Furthermore, the experimental investigations present guidelines for choosing VCSEL sizes, bias currents and modulation voltages depending on the requirements in terms of power consumption, expected life span, bit-error rate, communication signal quality.

Physically distributing the antenna elements of a MIMO communication system can increase the signal quality, coverage and reliability, especially when the channels between different transmitters and receivers are highly correlated. One of the major difficulties of forming such systems is to provide RF-phase coherency between separated antenna elements. SDoF provides this naturally due to digital up-conversion performed at a central location with the same

clock/signal source. A testbed is implemented in order to demonstrate the capabilities of SDoF for forming distributed antenna systems. It provides very good RF-phase coherency between different antenna elements and high flexibility due to its all-digital nature. The testbed not only exhibits the advantages of SDoF but is also a powerful platform for conducting measurements and analysis of distributed MIMO communication systems in real environments.

SDoF provides many benefits as presented throughout out the thesis. However, for SDoF to be realizable in real-time networks, an uplink solution is also required. Most of the current methods, would imperil many benefits of SDoF in terms of complexity, cost, flexibility and scalability. The work in this thesis proposes a suitable uplink architecture for SDoF systems. The method quantizes the received RF signal at the RRH directly in to a binary stream by comparing to a tailored reference signal. The reference signal is generated at the central unit and transferred through the downlink during the uplink phase. Hence, the reference signal properties can be adjusted according to the received signal. The proposed architecture is highly suitable for realization of future distributed wireless communication systems due to its all-digital, low-complexity nature.

In summary, this thesis has evaluated the potential and limitations of SDoF communication links both from an optical component and wireless communication perspective. A SDoF based testbed using commercial optical components is designed and implemented and used to evaluate emerging distributed MIMO wireless communication solutions. An ultra-high-speed SDoF link using Chalmers in-house components is also implemented to evaluate the limits of the SDoF concept. All of these investigations show that SDoF is a powerful technique which can be implemented in various scenarious from distributed MIMO to ultra-high-speed communication systems.

5.1 Future Work

The following areas are interesting to explore in future research.

5.1.1 mm-Wave Testbed

The current implementation of the distributed MIMO testbed supports carrier frequencies up to 5-GHz. However, 5G frequency range 2 (FR2) will operate at frequency bands above 24 GHz. A distributed MIMO testbed with capabilities of transmission at mm-Wave will be highly beneficial for experimental studies at an early stage. There are different solutions to realize a mm-Wave SDoF distributed MIMO testbed. One possibility is to directly convert the signal to the communication frequency, which would require very high speed sampling rates at the central unit. In [42] a single-link RF SDoF is demonstrated for mm-Wave communication, such structure can be developed further for multiple, centralized communication links. On the other hand, an intermediate frequency (IF) signal can be transmitted through the optical fiber as presented in [46]. This would require mixers and local oscillators at the remote radio head. The RF-phase coherency between remote radio heads can be provided through transmission of reference signals together with the IF signal. Another approach would be using optical heterodyning as presented in [34]. In this method the

signal is first upconverted to an intermediate frequency, and later the signal is shifted to desired operation frequency using optical combiners. One or more of these methods can be implemented and a mm-Wave distributed MIMO testbed can be achieved.

5.1.2 Real-time FPGA Implementation

Throughout the thesis, the sigma delta modulation is performed offline in MATLAB. For example, as presented in [37,38,42,43], a real-time implementation of sigma delta modulation together with all the other signal processing algorithms in the FPGA will turn the testbed in to a real-time communication system.

5.1.3 Positioning

Wireless communication signals can be utilized to estimate the position of an user equipment [131]. There are three main techniques to perform this: using the received signal strength (RSS) [132], using the angle-of-arrival (AOA) of the received signal [133], and using the propagation delay of the received signal [134,135]. Any of these methods can be implemented with the testbed, since it provides RF-phase coherency. It is very interesting to implement one (or more) of these methods to compare the effects of distributing the antenna elements for positioning.

5.1.4 MIMO Uplink

The proposed uplink method in Chapter 4 is demonstrated for a SISO system. Implementing it for all of the communication channels would result in a complete, time-domain duplex, distributed-MIMO testbed. This would enable study of the effect of non-ideal uplinks as opposed to the current implementation of the testbed.

The constant developments in digital and optical components, makes SDoF more feasible and cost-efficient for realizing wireless communication networks. For this reason, SDoF will stay as an *hot* research area for a long while. This will bring many other use-case possibilities, which are not covered here.

Acknowledgments

I think this is one of the hardest parts of writing this thesis, expressing my gratitude to the people who supported me during my doctoral studies, I don't think I can find enough words to express my thankfulness. Nevertheless, I will try my best!

First of all, I would like to start with my examiner, Prof. Herbert Zirath. Thank you for the opportunity to become a part of very inspiring group as Ph.D. student.

My deepest gratitude is to my main supervisor, Prof. Christian Fager, for his limitless support. No matter how busy you are with all the responsibilities you have, you always have time to supervise and have very fruitful discussions. I am very lucky, because I know I can always knock on your door and get your advice on anything. This hole journey has been very inspiring for me as becoming a researcher. Thank you!

I would like to thank Prof. Thomas Eriksson, my co-supervisor, for his support from the beginning of my doctoral studies. All our long, thorough discussions in signal processing field were very helpful. It is always relieving to know that I can have a meeting with you whenever I need!

Assoc. Prof. Johan Gustavsson, my co-supervisor, thank you very much for your time and your guidance about photonics and optical communication techniques. Your technical expertise improved the quality of my research.

Special thanks to Asst. Prof. Zhongxia Simon He. I really appreciate our discussions and your guidance. It is always a pleasure to discuss with you regardless of the topic.

I also would like to thank Prof. Henk Wymeersch and Furkan Keskin for our collaboration during the localization studies.

I am particularly grateful to all my colleagues for creating such a welcoming and fun working environment. Especially, Ahmed Hassona, Frida Strömbeck, Hamza Nachouane, Han Zhou, Jose-Ramon Perez-Cisneros, Olivier Auriacombe, Sining An, William Hallberg; it is a pleasure to be your friend and thanks for making the office-life way funnier!

Necla, you were there to support me every single time I struggled in my life. I could write a book to acknowledge you, yet I need to express my gratitude in couple of lines. So, I prefer to say, I love you!

I don't think there are enough words to express my gratitude to my parents. Their support throughout my life enabled me to write a doctoral thesis. Melahat and Ümit, thank you very much!

This work was financed by Swedish Research Council through grant number 2015-04000.

Bibliography

[1] "Ericsson Mobility Report," Ericsson AB, Tech. Rep., June 2020.

[2] "The 5g consumer business case," Ericsson, Tech. Rep., 2018.

[3] "Common public radio interface." [Online]. Available: http://www.cpri.info/

[4] M. Shafi, A. F. Molisch, P. J. Smith, T. Haustein, P. Zhu, P. De Silva, F. Tufvesson, A. Benjebbour, and G. Wunder, "5G: A tutorial overview of standards, trials, challenges, deployment, and practice," *IEEE Journal on Selected Areas in Communications*, vol. 35, no. 6, pp. 1201–1221, 2017.

[5] N. Argyris, G. Giannoulis, K. Kanta, N. Iliadis, C. Vagionas, S. Papaioannou, G. Kalfas, D. Apostolopoulos, C. Caillaud, H. Debrégeas, N. Pleros, and H. Avramopoulos, "A 5G mmwave fiber-wireless IFoF analog mobile fronthaul link with up to 24-Gb/s multiband wireless capacity," *Journal of Lightwave Technology*, vol. 37, no. 12, pp. 2883–2891, 2019.

[6] C. Ranaweera, E. Wong, A. Nirmalathas, C. Jayasundara, and C. Lim, "5G C-RAN with optical fronthaul: An analysis from a deployment perspective," *Journal of Lightwave Technology*, vol. 36, no. 11, pp. 2059–2068, 2018.

[7] D. M. Fye, "Design of fiber optic antenna remoting links for cellular radio applications," in *40th IEEE Conference on Vehicular Technology*, May 1990, pp. 622–625.

[8] A. J. Cooper, "'fibre/radio' for the provision of cordless/mobile telephony services in the access network," *Electronics Letters*, vol. 26, no. 24, pp. 2054–2056, Nov 1990.

[9] A. J. Seeds and K. J. Williams, "Microwave photonics," *J. Lightw. Technol*, vol. 24, no. 12, pp. 4628–4641, Dec 2006.

[10] A. Nirmalathas, P. A. Gamage, C. Lim, D. Novak, and R. Waterhouse, "Digitized radio-over-fiber technologies for converged optical wireless access network," *J. Lightw. Technol*, vol. 28, no. 16, pp. 2366–2375, Aug 2010.

[11] G. Chang, A. Chowdhury, , and G. Ellinas, "Architectures and technologies for very high throughput in-building wireless services using radio-over-fiber networks," in *2009 IEEE/LEOS Summer Topical Meeting*, July 2009, pp. 37–38.

[12] R. M. Borges, T. R. R. Marins, M. S. B. Cunha, H. R. D. Filgueiras, I. F. da Costa, R. N. da Silva, D. H. Spadoti, L. L. Mendes, and A. C. Sodré, "Integration of a GFDM-based 5G transceiver in a GPON using radio over fiber technology," *J. Lightw. Technol.*, vol. 36, no. 19, pp. 4468–4477, Oct 2018.

[13] Y. Li, I. A. Hemadeh, M. El-Hajjar, and L. Hanzo, "Radio over diber downlink design for spatial modulation and multi-set space-time shift-keying," *IEEE Access*, vol. 6, pp. 21 812–21 827, 2018.

[14] A. Delmade, C. Browning, A. Farhang, N. Marchetti, L. E. Doyle, R. D. Koilpillai, L. P. Barry, and D. Venkitesh, "Performance analysis of analog IF over fiber fronthaul link with 4G and 5G coexistence," *IEEE J. Opt. Commun. Netw*, vol. 10, no. 3, pp. 174–182, March 2018.

[15] J. Nanni, J. Polleux, C. Algani, S. Rusticelli, F. Perini, and G. Tartarini, "VCSEL-based radio-over-G652 fiber system for short-/medium-range MFH solutions," *J. Lightw. Technol*, vol. 36, no. 19, pp. 4430–4437, Oct 2018.

[16] M. Noweir, Q. Zhou, A. Kwan, R. Valivarthi, M. Helaoui, W. Tittel, and F. M. Ghannouchi, "Digitally linearized radio-over fiber transmitter architecture for cloud radio access network's downlink," *IEEE Transactions on Microwave Theory and Techniques*, vol. 66, no. 7, pp. 3564–3574, 2018.

[17] C. Lim, A. Nirmalathas, M. Bakaul, P. Gamage, K. Lee, Y. Yang, D. Novak, and R. Waterhouse, "Fiber-wireless networks and subsystem technologies," *Journal of Lightwave Technology*, vol. 28, no. 4, pp. 390–405, 2010.

[18] T. Kurniawan, A. Nirmalathas, C. Lim, D. Novak, and R. Waterhouse, "Performance analysis of optimized millimeter-wave fiber radio links," *IEEE Trans. Microw. Theory Techn.*, vol. 54, no. 2, pp. 921–928, Feb 2006.

[19] C. Lim, A. Nirmalathas, K. Lee, D. Novak, and R. Waterhouse, "Intermodulation distortion improvement for fiber–radio applications incorporating OSSB+C modulation in an optical integrated-access environment," *Journal of Lightwave Technology*, vol. 25, no. 6, pp. 1602–1612, 2007.

[20] U. Gliese, S. Norskov, and T. N. Nielsen, "Chromatic dispersion in fiber-optic microwave and millimeter-wave links," *IEEE Transactions on Microwave Theory and Techniques*, vol. 44, no. 10, pp. 1716–1724, 1996.

[21] P. A. Gamage, A. Nirmalathas, C. Lim, D. Novak, and R. Waterhouse, "Design and analysis of digitized RF-over-fiber links," *Journal of Lightwave Technology*, vol. 27, no. 12, pp. 2052–2061, 2009.

[22] A. Nirmalathas, P. A. Gamage, C. Lim, D. Novak, R. Waterhouse, and Y. Yang, "Digitized RF transmission over fiber," *IEEE Microwave Magazine*, vol. 10, no. 4, pp. 75–81, 2009.

[23] D. M. Akos, M. Stockmaster, J. B. Y. Tsui, and J. Caschera, "Direct bandpass sampling of multiple distinct RF signals," *IEEE Transactions on Communications*, vol. 47, no. 7, pp. 983–988, 1999.

[24] D. Novak, R. B. Waterhouse, A. Nirmalathas, C. Lim, P. A. Gamage, T. R. Clark, M. L. Dennis, and J. A. Nanzer, "Radio-over-fiber technologies for emerging wireless systems," *IEEE Journal of Quantum Electronics*, vol. 52, no. 1, pp. 1–11, 2016.

[25] H. Jung, K. W. Lee, J. Kim, Y. Kwon, and J. H. Park, "Performance comparison of analog and digitized RoF systems with nonlinear channel condition," *IEEE Photon. Technol. Lett.*, vol. 28, no. 6, pp. 661–664, March 2016.

[26] "Open base station architecture initiative." [Online]. Available: http://www.obsai.com/

[27] L. M. Pessoa, J. S. Tavares, D. Coelho, and H. M. Salgado, "Experimental evaluation of a digitized fiber-wireless system employing sigma delta modulation," *Optics Express*, vol. 22, no. 14, p. 17508, jul 2014.

[28] L. Breyne, G. Torfs, X. Yin, P. Demeester, and J. Bauwelinck, "Comparison between analog radio-over-fiber and sigma delta modulated radio-over-fiber," *IEEE Photonics Technology Letters*, vol. 29, no. 21, pp. 1808–1811, Nov 2017.

[29] R. Schreier and G. C. Temes, *Understanding Delta-Sigma Data Converters*, 1st ed. Hoboken N.J: John Wiley & Sons, 2004.

[30] S. Hein and A. Zakhor, "On the stability of sigma delta modulators," *IEEE Trans. Signal Process.*, vol. 41, pp. 2322–2348, 1993.

[31] W. L. Lee, "A novel higher order interpolative modulator topology for high resolution oversampling A/D converters," Master's thesis, Massachusetts Institute of Technology, Cambridge, MA, 1987.

[32] K. C. . Chao, S. Nadeem, W. L. Lee, and C. G. Sodini, "A higher order topology for interpolative modulators for oversampling A/D converters," *IEEE Transactions on Circuits and Systems*, vol. 37, no. 3, pp. 309–318, March 1990.

[33] S. Jang, G. Jo, J. Jung, B. Park, and S. Hong, "A digitized IF-over-fiber transmission based on low-pass delta-sigma modulation," *IEEE Photonics Technology Letters*, vol. 26, no. 24, pp. 2484–2487, 2014.

[34] A. Lorences-Riesgo, S. S. Pereira, D. C. Dinis, J. Vieira, A. S. R. Oliveira, and P. P. Monteiro, "Real-time fpga-based delta-sigma-modulation transmission for 60 GHz radio-over-fiber fronthaul," in *2018 European Conference on Optical Communication (ECOC)*, 2018, pp. 1–3.

[35] J. M. B. Oliveira, L. M. Pessoa, D. Coelho, J. S. Tavares, and H. M. Salgado, "Digitised radio techniques for fibre-wireless applications," in *2014 16th International Conference on Transparent Optical Networks (ICTON)*, July 2014, pp. 1–4.

[36] S. Hori, T. Yamase, M. Tanio, T. Kaneko, N. Tawa, K. Motoi, and K. Kunihiro, "A digital radio-over-fiber downlink system based on envelope delta-sigma modulation for multi-band/mode operation," in *2016 IEEE MTT-S International Microwave Symposium (IMS)*, May 2016, pp. 1–4.

[37] R. F. Cordeiro, A. S. R. Oliveira, and J. Vieira, "All-digital transmitter with RoF remote radio head," in *2014 IEEE MTT-S International Microwave Symposium (IMS2014)*, 2014, pp. 1–4.

[38] C. Wu, H. Li, J. Van Kerrebrouck, L. Breyne, L. Bogaert, P. Demeester, and G. Torfs, "Real-time 4×3.5 Gbps sigma delta radio-over-fiber for a low-cost 5G C-RAN downlink," in *2018 European Conference on Optical Communication (ECOC)*, 2018, pp. 1–3.

[39] J. Wang, Z. Yu, K. Ying, J. Zhang, F. Lu, M. Xu, L. Cheng, X. Ma, and G. Chang, "Digital mobile fronthaul based on delta-sigma modulation for 32 LTE carrier aggregation and FBMC signals," *IEEE J. Opt. Commun. Netw*, vol. 9, no. 2, pp. A233–A244, Feb 2017.

[40] J. Wang, Z. Jia, L. A. Campos, L. Cheng, C. Knittle, and G. Chang, "Delta-sigma digitization and optical coherent transmission of DOCSIS 3.1 signals in hybrid fiber coax networks," *J. Lightw. Technol.*, vol. 36, no. 2, pp. 568–579, Jan 2018.

[41] A. Frappe, A. Flament, B. Stefanelli, A. Kaiser, and A. Cathelin, "An all-digital RF signal generator using high-speed $\Delta\Sigma$ modulators," *IEEE Journal of Solid-State Circuits*, vol. 44, no. 10, pp. 2722–2732, 2009.

[42] H. Li, M. Verplaetse, J. Verbist, J. Van Kerrebrouck, L. Breyne, C. Wu, L. Bogaert, B. Moeneclaey, X. Yin, J. Bauwelinck, P. Demeester, and G. Torfs, "Real-time 100-GS/s sigma-delta modulator for all-digital radio-over-fiber transmission," *Journal of Lightwave Technology*, vol. 38, no. 2, pp. 386–393, 2020.

[43] C. Wu, H. Li, O. Caytan, J. Van Kerrebrouck, L. Breyne, J. Bauwelinck, P. Demeester, and G. Torfs, "Distributed multi-user MIMO transmission using real-time sigma-delta-over-fiber for next generation fronthaul interface," *Journal of Lightwave Technology*, vol. 38, no. 4, pp. 705–713, 2020.

[44] J. Wang, Z. Jia, L. A. Campos, and C. Knittle, "Real-time demonstration of 5-GSa/s delta-sigma digitization for ultra-wide-bandwidth LTE and 5G signals in next generation fronthaul interface," in *2018 European Conference on Optical Communication (ECOC)*, 2018, pp. 1–3.

[45] ——, "Delta-sigma modulation for next generation fronthaul interface," *Journal of Lightwave Technology*, vol. 37, no. 12, pp. 2838–2850, 2019.

[46] C. Wu, H. Li, J. Van Kerrebrouck, A. Vandierendonck, I. L. de Paula, L. Breyne, O. Caytan, S. Lemey, H. Rogier, J. Bauwelinck, P. Demeester, and G. Torfs, "Distributed antenna system using sigma-delta intermediate-frequency-over-fiber for frequency bands above 24 GHz," *Journal of Lightwave Technology*, vol. 38, no. 10, pp. 2765–2773, 2020.

[47] T. Hung, J. Rode, L. E. Larson, and P. M. Asbeck, "Design of H-Bridge Class-D power amplifiers for digital pulse modulation transmitters," *IEEE Transactions on Microwave Theory and Techniques*, vol. 55, no. 12, pp. 2845–2855, 2007.

[48] M. Nielsen and T. Larsen, "A transmitter architecture based on delta–sigma modulation and switch-mode power amplification," *IEEE Transactions on Circuits and Systems II: Express Briefs*, vol. 54, no. 8, pp. 735–739, 2007.

[49] K. Kitamura, S. Sasaki, Y. Matsuya, and T. Douseki, "Optical wireless digital-sound transmission system with 1-bit $\Delta\Sigma$-modulated visible light and spherical Si solar cells," *IEEE Sensors Journal*, vol. 10, no. 11, pp. 1753–1758, 2010.

[50] H. Qian, J. Chen, S. Yao, Z. Y. Zhang, H. Zhang, and W. Xu, "One-bit sigma-delta modulator for nonlinear visible light communication systems," *IEEE Photonics Technology Letters*, vol. 27, no. 4, pp. 419–422, 2015.

[51] J. Arias, P. Kiss, V. Prodanov, V. Boccuzzi, M. Banu, D. Bisbal, J. S. Pablo, L. Quintanilla, and J. Barbolla, "A 32-mW 320-MHz continuous-time complex delta-sigma ADC for multi-mode wireless-LAN receivers," *IEEE Journal of Solid-State Circuits*, vol. 41, no. 2, pp. 339–351, 2006.

[52] C. Wu, E. Alon, and B. Nikolić, "A wideband 400 MHz-to-4 GHz direct RF-to-digital multimode $\Delta\Sigma$ receiver," *IEEE Journal of Solid-State Circuits*, vol. 49, no. 7, pp. 1639–1652, 2014.

[53] S. Yan and E. Sanchez-Sinencio, "A continuous-time sigma-delta modulator with 88-dB dynamic range and 1.1-MHz signal bandwidth," *IEEE Journal of Solid-State Circuits*, vol. 39, no. 1, pp. 75–86, 2004.

[54] A. Jerng and C. G. Sodini, "A Wideband digital-RF modulator for high data rate transmitters," *IEEE Journal of Solid-State Circuits*, vol. 42, no. 8, pp. 1710–1722, 2007.

[55] N. V. Silva, A. S. R. Oliveira, and N. B. Carvalho, "Evaluation of pulse modulators for all-digital agile transmitters," in *2012 IEEE/MTT-S International Microwave Symposium Digest*, 2012, pp. 1–3.

[56] ——, "Design and optimization of flexible and coding efficient all-digital RF transmitters," *IEEE Transactions on Microwave Theory and Techniques*, vol. 61, no. 1, pp. 625–632, 2013.

[57] R. F. Cordeiro, A. S. R. Oliveira, J. Vieira, and T. O. e Silva, "Wideband all-digital transmitter based on multicore DSM," in *2016 IEEE MTT-S International Microwave Symposium (IMS)*, 2016, pp. 1–4.

[58] D. C. Dinis, R. F. Cordeiro, A. S. R. Oliveira, J. Vieira, and T. O. Silva, "Improving the performance of all-digital transmitter based on parallel delta-sigma modulators through propagation of state registers," in *2017 IEEE 60th International Midwest Symposium on Circuits and Systems (MWSCAS)*, 2017, pp. 1133–1137.

[59] M. Tanio, S. Hori, N. Tawa, T. Yamase, and K. Kunihiro, "An FPGA-based all-digital transmitter with 28-GHz time-interleaved delta-sigma modulation," in *2016 IEEE MTT-S International Microwave Symposium (IMS)*, 2016, pp. 1–4.

[60] M. Tanio, S. Hori, N. Tawa, and K. Kunihiro, "An FPGA-based all-digital transmitter with 9.6-GHz 2nd order time-interleaved delta-sigma modulation for 500-MHz bandwidth," in *2017 IEEE MTT-S International Microwave Symposium (IMS)*, 2017, pp. 149–152.

[61] M. Helaoui, S. Hatami, R. Negra, and F. M. Ghannouchi, "A novel architecture of delta-sigma modulator enabling all-digital multiband multistandard RF transmitters design," *IEEE Transactions on Circuits and Systems II: Express Briefs*, vol. 55, no. 11, pp. 1129–1133, 2008.

[62] S. Chung, Rui Ma, S. Shinjo, and K. H. Teo, "Inter-band carrier aggregation digital transmitter architecture with concurrent multi-band delta-sigma modulation using out-of-band noise cancellation," in *2015 IEEE MTT-S International Microwave Symposium*, 2015, pp. 1–4.

[63] S. Chung, R. Ma, S. Shinjo, H. Nakamizo, K. Parsons, and K. H. Teo, "Concurrent multiband digital outphasing transmitter architecture using multidimensional power coding," *IEEE Transactions on Microwave Theory and Techniques*, vol. 63, no. 2, pp. 598–613, 2015.

[64] K. Iga, "Surface-emitting laser-its birth and generation of new optoelectronics field," *IEEE J. Sel. Topics Quantum Electron*, vol. 6, no. 6, pp. 1201–1215, Nov 2000.

[65] D. K. Serkland, G. M. Peake, K. M. Geib, R. Lutwak, R. M. Garvey, M. Varghese, and M. Mescher, "VCSELs for atomic clocks," in *Vertical-Cavity Surface-Emitting Lasers X*, ser. Proc.SPIE, C. Lei and K. D. Choquette, Eds., vol. 6132, Feb. 2006, pp. 66–76.

[66] *VCSEL array-based light exposure system for laser printing*, vol. 6908, 2008.

[67] A. Extance, "Faces light up over VCSEL prospects," *SPIE Newsroom*, Apr. 2018.

[68] G. Totschnig, M. Lackner, R. Shau, M. Ortsiefer, J. Rosskopf, M. Amann, and F. Winter, "High-speed vertical-cavity surface-emitting laser (VCSEL) absorption spectroscopy of ammonia (NH3) near 1.54 μm," *Applied Physics B*, vol. 76, no. 5, pp. 603–608, May 2003.

[69] *Volume production of polarization controlled single-mode VCSELs*, vol. 6908, 2008.

[70] F. Koyama, "Recent advances of VCSEL photonics," *J. Lightw. Technol.*, vol. 24, no. 12, pp. 4502–4513, Dec 2006.

[71] P. Westbergh, R. Safaisini, E. Haglund, J. S. Gustavsson, A. Larsson, M. Geen, R. Lawrence, and A. Joel, "High-speed oxide confined 850-nm VCSELs operating error-free at 40 Gb/s up to 85 C," *IEEE Photon. Technol. Lett*, vol. 25, no. 8, pp. 768–771, apr 2013.

[72] P. Westbergh, E. Haglund, E. Haglund, R. Safaisini, J. Gustavsson, and A. Larsson, "High-speed 850 nm VCSELs operating error free up to 57 Gbit/s," *Electronics Letters*, vol. 49, no. 16, pp. 1021–1023, aug 2013.

[73] J. A. Tatum, D. Gazula, L. A. Graham, J. K. Guenter, R. H. Johnson, J. King, C. Kocot, G. D. Landry, I. Lyubomirsky, A. N. MacInnes, E. M. Shaw, K. Balemarthy, R. Shubochkin, D. Vaidya, M. Yan, and F. Tang, "VCSEL-based interconnects for current and future data centers," *J. Lightw. Technol.*, vol. 33, no. 4, pp. 727–732, Feb 2015.

[74] X. Zhang, W. Pan, J. Chen, and H. Zhang, "Theoretical calculation of turn-on delay time of VCSEL and effect of carriers recombination," *Optics & Laser Technology*, vol. 39, no. 5, pp. 997–1001, jul 2007.

[75] W. H. Hofmann, P. Moser, and D. Bimberg, "Energy-efficient VCSELs for interconnects," *IEEE Photon. J.*, vol. 4, no. 2, pp. 652–656, April 2012.

[76] P. Moser, J. A. Lott, and D. Bimberg, "Energy efficiency of directly modulated oxide-confined high bit rate 850-nm VCSELs for optical interconnects," *IEEE J. Sel. Topics Quantum Electron*, vol. 19, no. 4, pp. 1 702 212–1 702 212, jul 2013.

[77] Q. Han, J. Luo, H. Shen, Q. Chen, and J. Qu, "A 2–6 GHz fully integrated switched filter bank for multiband wireless communication applications," in *2019 International Conference on Microwave and Millimeter Wave Technology (ICMMT)*, 2019, pp. 1–3.

[78] T. Canning, P. J. Tasker, and S. C. Cripps, "Continuous mode power amplifier design using harmonic clipping contours: Theory and practice," *IEEE Trans. Microw. Theory Techn.*, vol. 62, no. 1, pp. 100–110, Jan 2014.

[79] A. Ghosh, A. Maeder, M. Baker, and D. Chandramouli, "5G evolution: A view on 5G cellular technology beyond 3GPP release 15," *IEEE Access*, vol. 7, pp. 127 639–127 651, 2019.

[80] J. G. Andrews, X. Zhang, G. D. Durgin, and A. K. Gupta, "Are we approaching the fundamental limits of wireless network densification?" *IEEE Communications Magazine*, vol. 54, no. 10, pp. 184–190, 2016.

[81] G. Interdonato, E. Björnson, H. Quoc Ngo, P. Frenger, and E. G. Larsson, "Ubiquitous cell-free massive mimo communications," *EURASIP Journal on Wireless Communications and Networking*, vol. 2019, no. 1, p. 197, Aug 2019. [Online]. Available: https://doi.org/10.1186/s13638-019-1507-0

[82] C. Wu, H. Li, O. Caytan, J. Van Kerrebrouck, L. Breyne, J. Bauwelinck, P. Demeester, and G. Torfs, "Distributed multi-user MIMO transmission using real-time sigma-delta-over-fiber for next generation fronthaul interface," *Journal of Lightwave Technology*, vol. 38, no. 4, pp. 705–713, Feb 2020.

[83] H. Rastegarfar, T. Svensson, and N. Peyghambarian, "Optical layer routing influence on software-defined C-RAN survivability," *IEEE/OSA Journal of Optical Communications and Networking*, vol. 10, no. 11, pp. 866–877, Nov 2018.

[84] I. A. Alimi, A. L. Teixeira, and P. P. Monteiro, "Toward an efficient C-RAN optical fronthaul for the future networks: A tutorial on technologies, requirements, challenges, and solutions," *IEEE Communications Surveys Tutorials*, vol. 20, no. 1, pp. 708–769, Firstquarter 2018.

[85] D. Chizhik, G. Foschini, M. Gans, and R. Valenzuela, "Keyholes, correlations, and capacities of multielement transmit and receive antennas," *IEEE Trans. Wireless Commun.*, vol. 1, no. 2, pp. 361–368, apr 2002.

[86] Chen-Nee Chuah, J. Kahn, and D. Tse, "Capacity of multi-antenna array systems in indoor wireless environment," in *IEEE GLOBECOM 1998 (Cat. NO. 98CH36250)*, vol. 4. IEEE, pp. 1894–1899.

[87] D. Wang, J. Wang, X. You, Y. Wang, M. Chen, and X. Hou, "Spectral efficiency of distributed MIMO systems," *IEEE Journal on Selected Areas in Communications*, vol. 31, no. 10, pp. 2112–2127, 2013.

[88] M. Matthaiou, C. Zhong, M. R. McKay, and T. Ratnarajah, "Sum rate analysis of ZF receivers in distributed MIMO systems," *IEEE Journal on Selected Areas in Communications*, vol. 31, no. 2, pp. 180–191, 2013.

[89] A. Saleh, A. Rustako, and R. Roman, "Distributed antennas for indoor radio communications," *IEEE Trans. Commun*, vol. 35, no. 12, pp. 1245–1251, dec 1987.

[90] M. Clark, T. Willis, L. Greenstein, A. Rustako, V. Erceg, and R. Roman, "Distributed versus centralized antenna arrays in broadband wireless networks," in *IEEE VTS 53rd Vehicular Technology Conference, Spring 2001. Proceedings (Cat. No.01CH37202)*, vol. 1. IEEE, pp. 33–37.

[91] Shidong Zhou, Ming Zhao, Xibin Xu, Jing Wang, and Yan Yao, "Distributed wireless communication system: a new architecture for future public wireless access," *IEEE Communications Magazine*, vol. 41, no. 3, pp. 108–113, mar 2003.

[92] Wonil Roh and A. Paulraj, "Outage performance of the distributed antenna systems in a composite fading channel," in *Proceedings IEEE 56th Vehicular Technology Conference*, vol. 3. IEEE, pp. 1520–1524.

[93] ——, "MIMO channel capacity for the distributed antenna," in *Proceedings IEEE 56th Vehicular Technology Conference*, vol. 2. IEEE, pp. 706–709.

[94] Z. Liu and L. Dai, "A comparative study of downlink MIMO cellular networks with co-located and distributed base-station antennas," *IEEE Trans. Wireless Commun.*, vol. 13, no. 11, pp. 6259–6274, nov 2014.

[95] H. Q. Ngo, A. Ashikhmin, H. Yang, E. G. Larsson, and T. L. Marzetta, "Cell-free massive MIMO versus small cells," *IEEE Trans. Wireless Commun.*, vol. 16, no. 3, pp. 1834–1850, mar 2017.

[96] H. V. Balan, R. Rogalin, A. Michaloliakos, K. Psounis, and G. Caire, "AirSync: Enabling distributed multiuser MIMO with full spatial multiplexing," *IEEE/ACM Trans. Netw.*, vol. 21, no. 6, pp. 1681–1695, dec 2013.

[97] H. Rahul, S. Kumar, and D. Katabi, "MegaMIMO: Scaling Wireless Capacity with User Demands," in *ACM SIGCOMM 2012*, Helsinki, Finland, August 2012.

[98] X. Zhang, K. Sundaresan, M. A. A. Khojastepour, S. Rangarajan, and K. G. Shin, "NEMOx: Scalable network MIMO for wireless networks," in *Proceedings of the 19th Annual International Conference on Mobile Computing & Networking*, ser. MobiCom '13. New York, NY, USA: ACM, 2013, pp. 453–464.

[99] V. Yenamandra and K. Srinivasan, "Vidyut: Exploiting power line infrastructure for enterprise wireless networks," in *Proceedings of the 2014 ACM Conference on SIGCOMM*, ser. SIGCOMM '14. New York, NY, USA: ACM, 2014, pp. 595–606.

[100] E. Hamed, H. Rahul, M. A. Abdelghany, and D. Katabi, "Real-time distributed MIMO systems," in *Proceedings of the 2016 ACM SIGCOMM Conference*, ser. SIGCOMM '16. New York, NY, USA: ACM, 2016, pp. 412–425.

[101] "Rice University WARP Project," 2012.

[102] "USRP, http://www.ettus.com, Ettus Inc."

[103] "Zedboard, http://zedboard.org , AVNET."

[104] "AD-FMCOMMS-EBZ, http://www.analog.com , Analog Devices."

[105] "NI-5791, http://www.ni.com, National Instruments."

[106] "Zinwave, http://www.zinwave.com , Zinwave."

[107] "pCell, https://www.artemis.com/pcell , Artemis."

[108] G. Caire and S. Shamai, "On the achievable throughput of a multiantenna Gaussian broadcast channel," *IEEE Trans. Inf. Theory*, vol. 49, no. 7, pp. 1691–1706, jul 2003.

[109] S. Roy and P. Fortier, "Maximal-ratio combining architectures and performance with channel estimation based on a training sequence," *IEEE Transactions on Wireless Communications*, vol. 3, no. 4, pp. 1154–1164, 2004.

[110] X. Lu, P. Wang, D. Niyato, D. I. Kim, and Z. Han, "Wireless networks with RF energy harvesting: A contemporary survey," *IEEE Communications Surveys Tutorials*, vol. 17, no. 2, pp. 757–789, Secondquarter 2015.

[111] T. D. Ponnimbaduge Perera, D. N. K. Jayakody, S. K. Sharma, S. Chatzinotas, and J. Li, "Simultaneous wireless information and power transfer (SWIPT): Recent advances and future challenges," *IEEE Communications Surveys Tutorials*, vol. 20, no. 1, pp. 264–302, Firstquarter 2018.

[112] L. R. Varshney, "Transporting information and energy simultaneously," in *2008 IEEE International Symposium on Information Theory*, July 2008, pp. 1612–1616.

[113] F. Yuan, S. Jin, Y. Huang, K. Wong, Q. T. Zhang, and H. Zhu, "Joint wireless information and energy transfer in massive distributed antenna systems," *IEEE Communications Magazine*, vol. 53, no. 6, pp. 109–116, 2015.

[114] ——, "Joint wireless information and energy transfer in massive distributed antenna systems," *IEEE Communications Magazine*, vol. 53, no. 6, pp. 109–116, 2015.

[115] A. Salem, L. Musavian, and K. A. Hamdi, "Wireless power transfer in distributed antenna systems," *IEEE Transactions on Communications*, vol. 67, no. 1, pp. 737–747, Jan 2019.

[116] X. Zhou, R. Zhang, and C. K. Ho, "Wireless information and power transfer: Architecture design and rate-energy tradeoff," *IEEE Transactions on Communications*, vol. 61, no. 11, pp. 4754–4767, 2013.

[117] (2020) Powercast P21xxcsr-EVB. [Online]. Available: https://www.powercastco.com/wp-content/uploads\/2016/10/P21XXCSR-EVB-Datasheet-v2.1.pdf

[118] E. Kwiatkowski, C. T. Rodenbeck, T. Barton, and Z. Popović, "Power-combined rectenna array for X-Band wireless power transfer," in *2020 IEEE/MTT-S International Microwave Symposium (IMS)*, 2020, pp. 992–995.

[119] U. Habib, A. E. Aighobahi, T. Quinlan, S. D. Walker, and N. J. Gomes, "Analog radio-over-fiber supported increased RAU spacing for 60 GHz distributed MIMO employing spatial diversity and multiplexing," *Journal of Lightwave Technology*, vol. 36, no. 19, pp. 4354–4360, 2018.

[120] W. B. Bridges and J. H. Schaffner, "Distortion in linearized electrooptic modulators," *IEEE Transactions on Microwave Theory and Techniques*, vol. 43, no. 9, pp. 2184–2197, 1995.

[121] Y.-T. Moon, J. W. Jang, W.-K. Choi, and Y.-W. Choi, "Simultaneous noise and distortion reduction of a broadband optical feedforward transmitter for multi-service operation in radio-over-fiber systems," *Opt. Express*, vol. 15, no. 19, pp. 12 167–12 173, Sep 2007. [Online]. Available: http://www.opticsexpress.org/abstract.cfm?URI=oe-15-19-12167

[122] J. Ning, Y. Dai, F. Yin, J. Li, Q. Lv, and K. Xu, "Digital linearization for broadband multicarrier analog photonic link incorporating

downconversion," *Optical Engineering*, vol. 55, no. 3, pp. 1 – 6, 2015. [Online]. Available: https://doi.org/10.1117/1.OE.55.3.031102

[123] W. Zhai, A. Wen, and D. Shan, "Multidimensional optimization of a radio-over-fiber link," *IEEE Transactions on Microwave Theory and Techniques*, pp. 1–1, 2020.

[124] M. Sung, J. Kim, E. Kim, S. Cho, Y. Won, B. Lim, S. Pyun, J. K. Lee, and J. H. Lee, "5G trial services demonstration: IFoF-based distributed antenna system in 28 GHz millimeter-wave supporting gigabit mobile services," *Journal of Lightwave Technology*, vol. 37, no. 14, pp. 3592–3601, 2019.

[125] Y. Yang, C. Lim, and A. Nirmalathas, "Multichannel digitized RF-over-fiber transmission based on bandpass sampling and FPGA," *IEEE Transactions on Microwave Theory and Techniques*, vol. 58, no. 11, pp. 3181–3188, 2010.

[126] A. Prata, A. S. R. Oliveira, and N. B. Carvalho, "All-digital flexible uplink remote radio head for C-RAN," in *2016 IEEE MTT-S International Microwave Symposium (IMS)*, May 2016, pp. 1–4.

[127] S. Maier, X. Yu, H. Heimpel, and A. Pascht, "Wideband base station receiver with analog-digital conversion based on RF pulse width modulation," in *2013 IEEE MTT-S International Microwave Symposium Digest (MTT)*, 2013, pp. 1–3.

[128] A. Prata, A. S. R. Oliveira, and N. B. Carvalho, "An agile and wideband all-digital SDR receiver for 5G wireless communications," in *2015 Euromicro Conference on Digital System Design*, 2015, pp. 146–151.

[129] R. F. Cordeiro, A. Prata, A. S. R. Oliveira, J. M. N. Vieira, and N. B. De Carvalho, "Agile all-digital RF transceiver implemented in FPGA," *IEEE Transactions on Microwave Theory and Techniques*, vol. 65, no. 11, pp. 4229–4240, Nov 2017.

[130] B. Widrow, I. Kollar, and Ming-Chang Liu, "Statistical theory of quantization," *IEEE Transactions on Instrumentation and Measurement*, vol. 45, no. 2, pp. 353–361, 1996.

[131] G. Piccinni, G. Avitabile, G. Coviello, and C. Talarico, "Real-time distance evaluation system for wireless localization," *IEEE Transactions on Circuits and Systems I: Regular Papers*, vol. 67, no. 10, pp. 3320–3330, 2020.

[132] J. Koo and H. Cha, "Localizing WiFi access points using signal strength," *IEEE Communications Letters*, vol. 15, no. 2, pp. 187–189, 2011.

[133] D. Inserra and A. M. Tonello, "A frequency-domain LOS angle-of-arrival estimation approach in multipath channels," *IEEE Transactions on Vehicular Technology*, vol. 62, no. 6, pp. 2812–2818, 2013.

[134] Y. Qi, C. B. Soh, E. Gunawan, K. Low, and A. Maskooki, "An accurate 3D UWB hyperbolic localization in indoor multipath environment using iterative taylor-series estimation," in *2013 IEEE 77th Vehicular Technology Conference (VTC Spring)*, 2013, pp. 1–5.

[135] B. Jang and H. Kim, "Indoor positioning technologies without offline fingerprinting map: A survey," *IEEE Communications Surveys Tutorials*, vol. 21, no. 1, pp. 508–525, 2019.